

Article

Sedimentary and Diagenetic Controls across the Cretaceous—Paleogene Transition: New Paleoenvironmental Insights of the External Ionian Zone from the Pelagic Carbonates of the Gardiki Section (Epirus, Western Greece)

Leonidas Moforis ^{1,*}, George Kontakiotis ^{1,*}, Hammad Tariq Janjuhah ², Alexandra Zambetakis-Lekkas ¹, Dimitrios Galanakis ³, Panagiotis Paschos ³, Christos Kanellopoulos ^{3,4}, Sotirios Sboras ⁵, Evangelia Besiou ¹, Vasileios Karakitsios ¹ and Assimina Antonarakou ¹

¹ Department of Historical Geology and Paleontology, Faculty of Geology and Geoenvironment, National and Kapodistrian University of Athens, Panepistimiopolis, Zografou, 15784 Athens, Greece

² Department of Geology, Shaheed Benazir Bhutto University, Sheringal 18050, KPK, Pakistan

³ H.S.G.M.E.—Hellenic Survey of Geology and Mineral Exploration, 13677 Athens, Greece

⁴ Department of Mineralogy & Petrology, Faculty of Geology and Geoenvironment, National and Kapodistrian University of Athens, Panepistimiopolis, Zografou, 15784 Athens, Greece

⁵ Institute of Geodynamics, National Observatory of Athens, Lofos Nymphon, Thessio, 11810 Athens, Greece

* Correspondence: leonidasmoforis@gmail.com (L.M.); gkontak@geol.uoa.gr (G.K.)



Citation: Moforis, L.; Kontakiotis, G.; Janjuhah, H.T.; Zambetakis-Lekkas, A.; Galanakis, D.; Paschos, P.; Kanellopoulos, C.; Sboras, S.; Besiou, E.; Karakitsios, V.; et al. Sedimentary and Diagenetic Controls across the Cretaceous—Paleogene Transition: New Paleoenvironmental Insights of the External Ionian Zone from the Pelagic Carbonates of the Gardiki Section (Epirus, Western Greece). *J. Mar. Sci. Eng.* **2022**, *10*, 1948. <https://doi.org/10.3390/jmse10121948>

Academic Editor: Antoni Calafat

Received: 31 October 2022

Accepted: 29 November 2022

Published: 8 December 2022

Publisher's Note: MDPI stays neutral with regard to jurisdictional claims in published maps and institutional affiliations.



Copyright: © 2022 by the authors. Licensee MDPI, Basel, Switzerland. This article is an open access article distributed under the terms and conditions of the Creative Commons Attribution (CC BY) license (<https://creativecommons.org/licenses/by/4.0/>).

Abstract: Field investigation, biostratigraphic, paleoecological, and sedimentary microfacies analyses, as well as diagenetic processes characterization, were carried out in the Epirus region (Western Ionian Basin) to define the depositional environments and further decipher the diagenetic history of the Late Cretaceous–Early Paleocene carbonate succession in western continental Greece. Planktonic foraminiferal biostratigraphy of the studied carbonates revealed that the investigated part of the Gardiki section covers the Cretaceous–Paleogene (K–Pg) transition, partly reflecting the Senonian limestone and calciturbidites formations of the Ionian zone stratigraphy. Litho- and bio-facies analyses allowed for the recognition of three distinct depositional facies: (a) the latest Maastrichtian pelagic biomicrite mudstone with in situ planktonic foraminifera, radiolarians, and filaments, (b) a pelagic biomicrite packstone with abundant planktonic foraminifera at the K–Pg boundary, and (c) an early Paleocene pelagic biomicrite wackestone with veins, micritized radiolarians, and mixed planktonic fauna in terms of in situ and reworked (aberrant or broken) planktonic foraminifera. The documented sedimentary facies characterize a relatively low to medium energy deep environment, representing the transition from the deep basin to the deep shelf and the toe of the slope crossing the K–Pg boundary. Micropaleontological and paleoecological analyses of the samples demonstrate that primary productivity collapse is a key proximate cause of this extinction event. Additional petrographic analyses showed that the petrophysical behavior and reservoir characteristics of the study deposits are controlled by the depositional environment (marine, meteoric, and burial diagenetic) and further influenced by diagenetic processes such as micritization, compaction, cementation, dissolution, and fracturing.

Keywords: microfacies analysis; Senonian limestone formation; siliceous nodules; diagenetic processes; slope-to-basin pelagic carbonates; Ionian calciturbidites; hydrocarbon reservoirs; K–T foraminiferal extinction; stratigraphic correlations; paleoenvironmental reconstruction

1. Introduction

Carbonate systems are a major component of the Earth system since they host more than 25% of the marine life [1], play an essential role in the global carbon cycle, and thus the regulation of atmospheric CO₂ concentration [2], and further represent major reservoir rocks for water and hydrocarbon resources [3–5]. Furthermore, marine biogenic carbonates

are among the most important archives of the climate [6,7], since their biotic constituents reflect changes in ocean chemistry and associated hydroclimate parameters (e.g., sea surface temperature and salinity; [8–10]). In particular, deeply buried carbonate successions in foreland basinal settings overlain by thick siliciclastic sediments are prospective targets for hydrocarbon and geothermal exploration [11]. Therefore, prediction and investigation of carbonate distributions through space and time represents a challenging scientific issue [6,12], which is critical for carbonate reservoir studies and the understanding of past and future climate changes at both a regional and global scales.

During the Late Cretaceous–Early Paleocene, the Mediterranean Tethys (Neo-Tethys) Ocean was characterized by the dominance of carbonate sedimentation, as witnessed by a spread of pelagic marine carbonates in the deeper parts of the basin (including the slope deposits in the platform margins) and shallow limestones and dolomites in the platform belts [13–16]. These carbonate sediments show different biotic associations, sedimentary facies, and stratigraphic architectures depending on the variable environmental conditions across the entire basin. During that time, within the tectonostratigraphic regime of western Greece, the carbonate deposits of the Ionian basin provide an excellent example of the evolution of depositional sequences ranging from deep basin to rimmed carbonate shelf settings. Moreover, the role of biogenic silica in the formation of Late Cretaceous–Early Paleocene pelagic carbonates is critical [17] and gives a great economic and strategic importance to these deposits [18–20]. They have been considered the main reservoir successions and exploration targets for oil and gas in western Greece [19–24]. Due to their increasing importance as reservoir rocks, the investigation of carbonate-derived thin sections gave substantial impetus to facies analysis development, making parallel progress in related topics such as sequence stratigraphy and sedimentology. However, the Late Cretaceous to early Eocene evolution of this setting, including the nature and distribution of these deposits, along with their depositional mechanism and diagenetic processes, are still poorly constrained.

In the present study, we investigate the depositional and diagenetic processes as well as the microfacies types of the Late Cretaceous–Early Paleocene carbonates of the Gardiki section, which is in the Epirus region (western Ionian basin, Ioannina, Greece). This study defines, for the first time, the Cretaceous–Paleogene (K–Pg) boundary depositional evolution in this area, based mainly on litho-stratigraphic, reservoir petrophysical, and diagenetic characteristics in the external Ionian domain, considered as a significant hydrocarbon prolific basin in Western Greece [20–22,25]. This was accomplished by extensive sedimentological and microfacies analyses of the carbonate succession, considering the synthetic paleoenvironmental reconstruction of the area. Finally, this work has further implications for regional geology and a better understanding of the Ionian basin in Western Greece.

2. Study Area

2.1. Regional Geological Setting

Western Greece is dominated by the external zones of the Hellenides fold-and-thrust belt, divided into three tectonostratigraphic zones, namely the pre-Apulian, Ionian, and Gavrovo-Tripolis zones. At a regional scale, this Alpine belt records the initiation, development, and final destruction of the southeastern margin of the Tethys Ocean and the consequent continent–continent collision between the Apulian and the Pelagonian microcontinents to the east [26,27]. On a local scale, the various sub-basins of the Hellenic Tethys margin have been inverted to produce the main Hellenic thrust sheet folded zones [28–30]. The Ionian zone, bounded westwards by the Ionian thrust and eastwards by the Gavrovo thrust, extends from Albania to the north, forms most of the Epirus region and parts of the Ionian islands, and continues southwards to Central Greece, Crete, and the Dodecanese (Figure 1). According to Aubouin [31] and Igrs-Ifp [32], the Ionian basin was subdivided into the Internal, Middle, and External sub-basins.

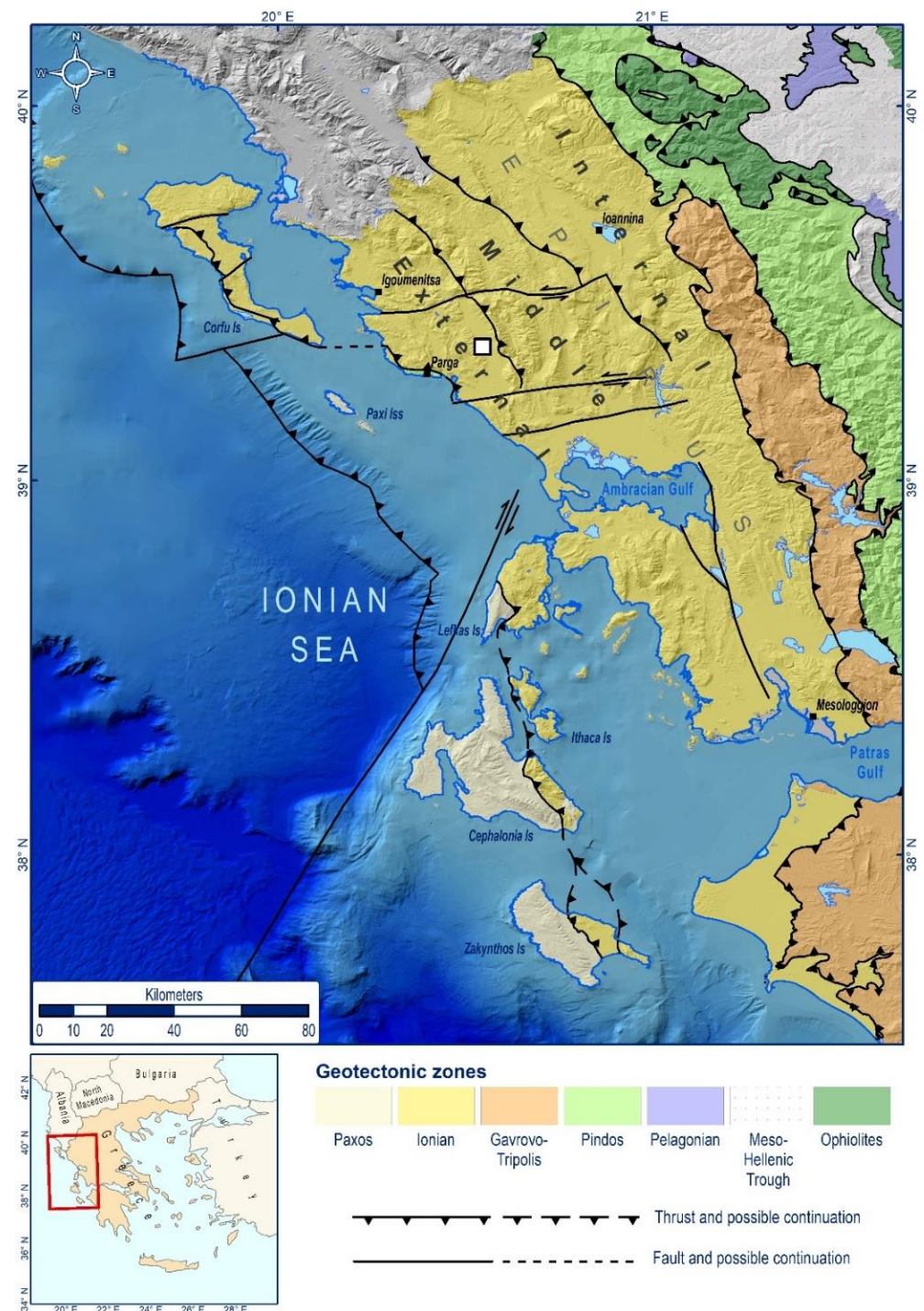


Figure 1. Geological map of the external Hellenides in Western Greece, illustrating the principal tectonostratigraphic zones: Pre-Apulian, Ionian, Gavrovo-Tripolis, and Pindos. The white square shows the location of the study section in external Ionian domain. Legend interpretations are presented in the inset.

2.2. Tectonostratigraphic Evolution of the Ionian Basin

The tectonostratigraphic evolution of the Ionian basin is reflected by the deposition of three distinct stratigraphic sequences indicative of different tectonic regimes. According to Karakitsios [22], these sequences are: the pre-rift, syn-rift, and post-rift (Figure 2).

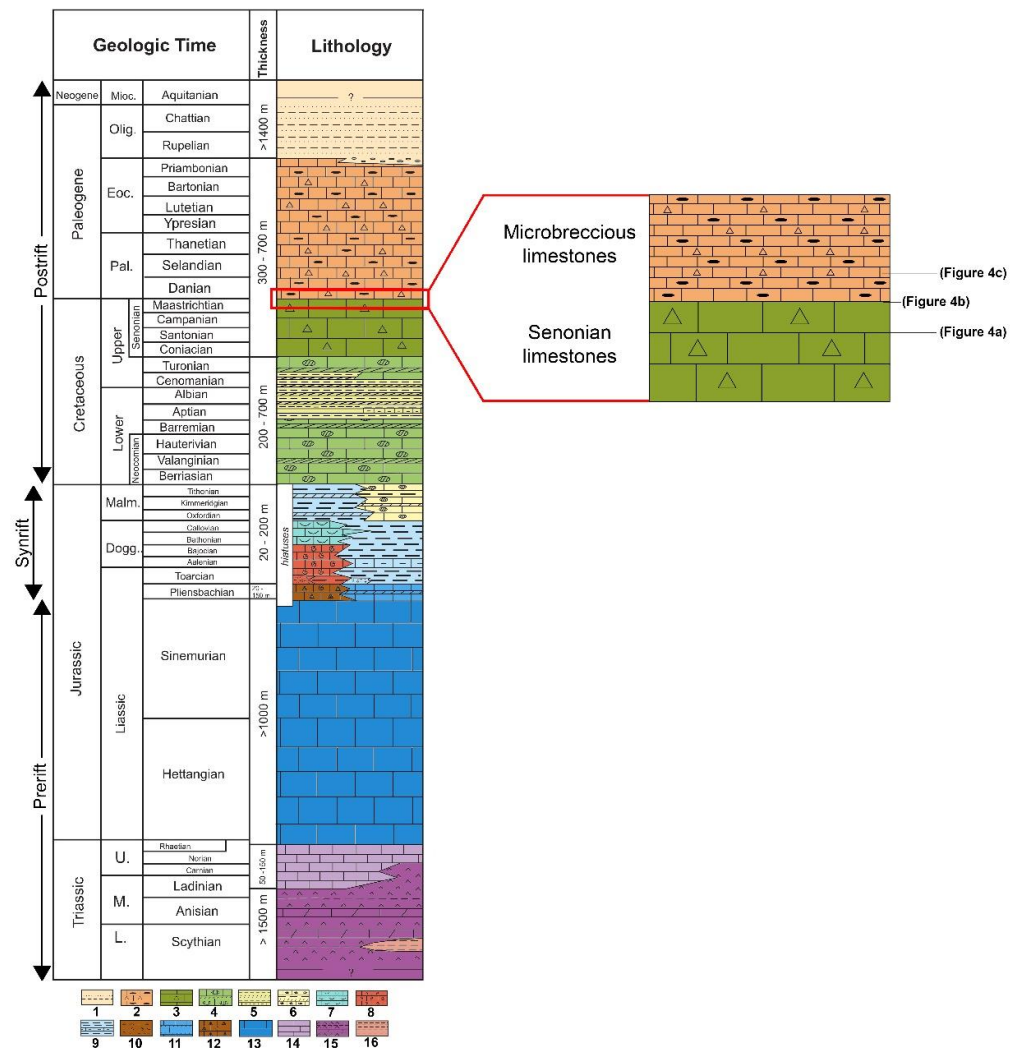


Figure 2. Synthetic lithostratigraphic column of the Ionian zone modified after [32], along with the correspondence of study section stratigraphy, as depicted in the enlarged view at the right, in which the position of the different litho-phases characteristic of the Cretaceous–Paleogene transition (corresponding to Figure 4a–c) is also highlighted. The colors in the lithostratigraphic column are consistent with the relevant colors of the International Chronostratigraphic Chart (v2020/01). (1) Shales and sandstones; (2) limestones with rare cherty intercalations, occasionally microbreccious; (3) pelagic limestones with clastic platform elements; (4) pelagic limestones with cherts; (5) cherty beds with shale and marl intercalations; (6) pelagic limestones with cherty nodules and marls; (7) pelagic limestones with bivalves; (8) pelagic, nodular red limestones with ammonites; (9) marly limestones and laminated marls; (10) conglomerates-breccias and marls with ammonites; (11) pelagic limestones with rare cherty intercalations; (12) external platform limestones with brachiopods and small ammonites in upper part; (13) platform limestones; (14) thin-bedded black limestones; (15) evaporites; (16) shales.

The oldest formation known in the pre-rift sequence is represented by the Lower to Middle Triassic evaporites, with a thickness greater than 2000 m, composed of anhydrites, gypsum, and halite, usually with interbeds of limestone and dolomite. The sequence is completed by the Late Ladinian–Rhaetian Foustapidima limestone [33] and by the overlying shallow water limestone of the Pantokrator formation of the Lower Jurassic (Hettangian to Sinemurian) age [34,35].

The syn-rift sequence begins with the Lower Jurassic (Pliensbachian) pelagic Siniais limestones and their lateral equivalent Louros limestones [36], overlain by Ammonitico Rosso and Limestones with filaments, laterally replaced and overlain by Posidonia beds [37].

The boundary between the Pantokrator and Sinia limestones is gradational. These formations correspond to the general deepening of the Ionian domain with the formation of the Ionian Basin. The structural differentiation separated the initial basin into smaller paleogeographic units with a half-graben geometry and remarkable different basin depths; in most cases, these units do not exceed 5 km across [37,38].

The post-rift sequence begins with the Lower Cretaceous (Berriasian-Turonian) pelagic Vigla limestones, whose deposition was synchronous throughout the Ionian Basin [35,39] and the laterally equivalent Vigla shales. The Vigla limestones cover the syn-rift structures [35], and in some cases, directly overlie the pre-rift units. Consequently, the base of the Vigla limestones formation represents the break-up unconformity of the post-rift sequence in the Ionian Basin. The Senonian limestones overlie the Vigla Formation and comprise two facies: (a) limestones with Globotruncanidae, and (b) microbrecciated intervals with limestones and rudist fragments within a calcareous cement containing pelagic fauna [20,21,23]. During the Paleocene-Eocene, the erosion of the Cretaceous carbonates from the adjacent Gavrovo (to the East) and Apulian platforms (to the West) provided the Ionian Basin with microbreccia or brecciated materials, known as Microbreccious limestones [19,20].

The Late Mesozoic to Eocene carbonate succession passes upwards to the flysch synorogenic sedimentation (siliciclastic turbidites), which began at the Eocene–Oligocene boundary and revealed progressively diminishing thicknesses from the internal to the external areas [34,35]. Until the Early Miocene, the basin was filled with submarine fan deposits in response to the movement of Pindos thrust, the compressional structures, and the deformation of the external Hellenides. As a result, it migrated westwards, uplifted the entire Hellenides orogenic belt, and developed a foreland basin at the edge of the Apulian microcontinent.

2.3. Senonian and Microbreccious Limestone Formations

In the present study, we exclusively focus on the K-Pg pelagic deposits of the Ionian basin consisted partly of the Senonian and microbreccious limestones (red box in Figure 2). These formations comprise of pelagic limestones with variable clastic platform elements (e.g., fragments of rudists and fine-grained microbrecciated intervals) and corresponds to a period of basinal sedimentation with significant variations of its lithological characteristics and sedimentary facies from the external (western) to the internal (eastern) parts of the Ionian basin [19,20] during the Late Cretaceous–Early Paleocene. According to Skourtsis-Coroneou et al. [40], their heterogeneity could be attributed to the presence of clastic limestones (e.g., floatstones-rudstones with a micritic matrix, biomicritic intercalations and rare cherty nodules) in the most external Ionian sub-basins, bioclastic wackestone to packstone intercalated with biomicrites in the middle sub-basins, and massive microbreccia containing rudists and coral fragments in the internal ones. Notably, the facies distribution of the Senonian reflects the separation of the Ionian Basin into a central area (the middle and outer parts of the Ionian Zone), characterized by deeper water sedimentation and two surrounding talus slopes issued from the western Gavrovo and Apulian platforms which provided the clastic carbonate material that was transported by turbidity currents into the Ionian basin [37]. Stratigraphically, although in some places these calciturbidites can be intercalated with the uppermost horizons of the underlying Vigla Limestone formation, in general they comfortably overlay the lower Cretaceous Vigla limestones and shales.

3. Materials and Methods

A total of 90 samples were collected from the Gardiki section (lat: 39°20'22.09" N, long: 20°33'5.63" E) in Epirus (western Greece), corresponding to the passage from the Late Cretaceous to the Paleocene. The fieldwork was conducted in October 2019, including field logging, measuring, and sampling, as well as additional observations made on the lithostratigraphic properties of the carbonates (i.e., color, lithological and textural variations, bed thickness, syn- and post-depositional features). The sampling resolution was variable along the section depending on the outcrop conditions, thickness, and lateral extent of each

carbonate unit. For samples B1 up to B39, the sampling resolution was 2.5 m, while for the rest of the samples (B40–B90) it was 0.2 m.

All selected samples were analyzed for microfacies (lithofacies and biofacies) and diagenetic characteristics to determine their precise age, paleoenvironmental depositional conditions, and diagenetic history. Thin sections were prepared both in the Historical Geology-Paleontology Laboratory (National and Kapodistrian University of Athens; NKUA) and at the Hellenic Survey of Geology and Mineral Exploration (H.S.G.M.E.), biostratigraphically and sedimentologically studied under a polarized LEICA DM LP microscope, and photos were performed with OLYMPUS UC30 Microscope Digital Camera. All thin sections (90 in total) were examined to determining different types of diagenetic processes performed on these deposits, and finally to evaluate the diagenetic history of the study formations.

The microfacies' definition and textural characters analysis of the carbonate rocks were defined according to Dunham [41] classification scheme, which were later modified by Embry and Klovan [42] and Flügel [43], based on the Standard Microfacies Types (SMF) in the Facies Zone (FZ) of the rimmed carbonate platform model. Depositional paleoenvironments were reconstructed based on the observed sedimentological characteristics during fieldwork and interpreted sedimentary facies analysis, and through comparison with additional outcropped data known from the existing literature on time equivalent deposits of the Ionian basin [18–20,44,45], as well as other environmental studies [46–54].

4. Results

4.1. Description of the Section and Field Observations

Figure 3 illustrates the location of the study part of Gardiki section, regarding the K-Pg carbonates in Epirus area.

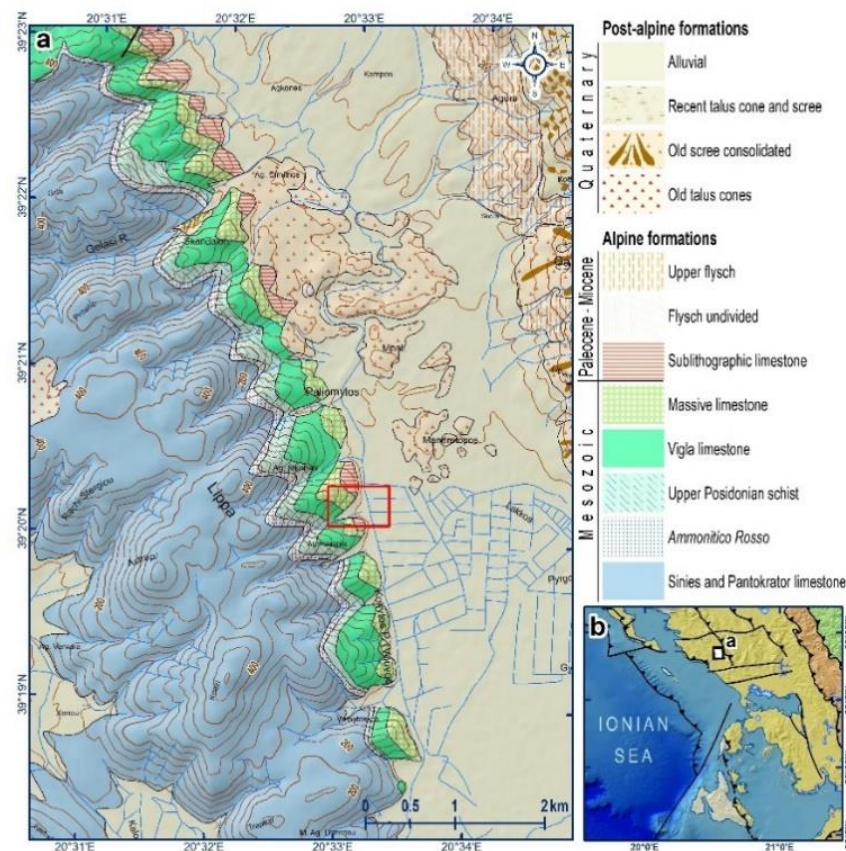


Figure 3. (a) General view of the study area based on the existing geological map. The red box indicates the study section. (b) Referenced map with the study lithostratigraphic units of the Ionian zone, as depicted in Figure 1. Geological data modified after [55].

The study part of Gardiki section consists of Late Cretaceous–Early Paleocene pelagic deposits, such as pelagic limestones and radiolarian chert horizons. The Senonian limestone formation in this area is mainly characterized by light-grey-to-yellowish limestones with abundant planktonic foraminifera, and more rare radiolarians. At the base of the section, thin-to-medium-bedded carbonate deposits are evident in rhythmic alternations with centimeter- to decimeter-thick cherts (Figure 4a). In the middle part of the section, the limestones become even thinner (Figure 4b), with the decrease in their thickness to be more evident when approaching the K-Pg boundary. Moreover, onwards up to the top of the section, the siliceous intervals occur very rarely as scarce thin chert intercalations (up to 5 cm thickness) and/or lenses within the dominant pelagic limestone unit. At the upper part of the section, a more uniform massive bioclastic limestone succession appears (Figure 4c). The lithology of this part of the section is described as solid, thick-bedded limestones that can be easily separated from the underlain medium-to-thin-bedded ones.

In the uppermost part of the section, reddish-to-brownish chert horizons, both nodular and bedded siliceous concretions, were observed. The siliceous nodules differ in size (up to 35 cm in diameter) and color (red to black), and appear in a variety of shapes, mostly sub-spherical, elongated-to-flattened, or mushroom ones (Figure 5a–c).

It is remarkable that all observed siliceous nodules are characterized by two or three distinct colors from the rim to the core, such as black to the periphery, rusty red brown to light red in the main body, and a thin blackish layer at the interior. This development in levels is probably due to differential mineralogic (quartz, moganite, chalcedony) and/or biogenic source (diatoms, radiolarian, or siliceous sponges) composition. The acute red color should be indicative of the advancement of certification, while the thin black layer at the interior and exterior is possibly related to diagenetic processes. Under such circumstances, the calcium carbonate can be replaced by waters rich in silica flowing through the rock and form diagenetic siliceous beds. Cherts formed in this way usually occurs as nodules within the carbonate succession, like the dark-colored nodules (Figure 5a), or thin siliceous beds as ribbon cherts (Figure 5b), mushroom-shaped masses (Figure 5c), lenses, or even the irregular in structure and size siliceous layers reported here. During field investigation, bedding parallel stylolites were also observed, which possess dissolution induced open longitudinal vugs and cavity-filling carbonate cement. Such features probably created during the nodules development and potentially act as a conduit for fluid (even for hydrocarbons) migration along their amplitude. Their presence should further reflect prolific source rocks through the reservoir properties (i.e., secondary porosity and permeability increase) increase of the hosted deposits through the fracturing.

4.2. Biostratigraphy and Paleoecology

The biostratigraphic analysis based on planktonic foraminifera showed that the study part of Gardiki section covers the boundary between the Late Cretaceous (Maastrichtian) and Early Paleocene (Danian) time span, exhibiting a well-preserved transition across the boundary. The age determination is in accordance with the geological map concerning the Ionian rock exposures in the Epirus area [55].

As described in detail in Table 1, the base of the section has a latest Maastrichtian age revealed by the presence of Globotrunciids and Heterohellicids in samples B1–B10. The middle part of the section (samples B11–B32) corresponds to the K-Pg boundary based on the coexistence of *Globotruncana stuarti* de Lapparent [56], *Globotruncana aegyptiaca* Nakkady [57], and Globigerinidae (Figure 7). Upwards up to the top (samples B33–B90), Globigeriniids are consistency present in higher abundance, while some Globotrunciids co-exist. However, the latter has a sporadic and highly variable presence and reveals a strong proliferation of altered tests (i.e., broken, dissolved) or aberrant forms, which are generally smaller in size within the Danian samples (samples B33–B90). In accordance with previous studies related to Danian reworking [58,59], such stratigraphic and size distribution peculiarities after the K-Pg boundary evidence that the Maastrichtian specimens are probably reworked. We note that additional stable isotopes on these species

and subsequent comparison of the isotopic values obtained below and above the K-Pg boundary will ensure if these species are in fact reworked or real Cretaceous survivors. However, such geochemical analyses could be considered as motivational for future work.



Figure 4. Outcrop images showing the different parts of Gardiki section corresponding to the Cretaceous–Paleogene transition. (a) Alterations of thin-to-medium-bedded limestones and cherts of Late Maastrichtian age, (b) Thin-bedded pelagic limestones corresponding to the K-Pg boundary, (c) Massive bioclastic limestone succession of early Paleocene age.



Figure 5. Reddish to brownish chert horizons. Siliceous nodules appear in a variety of shapes, mostly (a) sub-spherical, (b) elongated-to-flattened, or (c) mushroom types.

Table 1. Detailed description of the analyzed samples (thin sections), where depositional facies, lithology, formation, age, and depositional environments are presented.

Samples	Formation	Lithology	Facies Description	Figures (Lithology/Facies)	Depositional Environment	Energy Conditions	Chrono-Stratigraphy
B33–B90	Limestone with microbreccia	Massive bioclastic limestones with siliceous nodules	Bioclastic packstone enriched mostly on planktonic foraminifera or micritized radiolarians (SMF 3–4,10)	Figures 4c and 6c	Toe of slope (FZ3–4)	Medium energy	Early Paleocene (Danian)
B11–B32	Senonian	Thin-bedded limestones	Biomicrite wackestone–packstone with abundant planktonic foraminifera (SMF 2–3)	Figures 4b and 6b	Deep basin (FZ1) Deep shelf (FZ2)	Low to Medium energy	K–Pg boundary
B1–B10	Senonian	Thin- to medium-bedded limestones with cherts intercalations	Pelagic biomicrite mudstone (SMF 1–3)	Figures 4a and 6a	Deep basin (FZ1)	Low Energy	Late Cretaceous (Late Maastriichtian)

4.3. Sedimentary Microfacies Analysis

Within the Senonian limestone formation, we observed three distinct microfacies: (a) a pelagic biomicrite mudstone to wackestone with sparse planktonic foraminifera, radiolarians and filaments, which correspond to thin-to-medium-bedded deposits, (b) a pelagic biomicrite wackestone–packstone with abundant in situ planktonic foraminifera (both carenate and non-carenate forms), representing the thin-bedded bioclastic limestones of the K–Pg boundary, and (c) a pelagic biomicrite wackestone with both in situ and altered planktonic foraminifera and calcite veins of the massive carbonate unit (Figure 6).

4.4. Diagenetic Pathways and Processes

Diagenesis begins at the sediment–water interface, even if most of the changes occur after burial. Several distinct diagenetic characteristics were recognized in the K–Pg deposits based on sedimentological analysis. A specific diagenetic alteration condition was indicated by the diagenetic characteristics, which have a long-term effect on sedimentary rock. Micritization, compaction, cementation, dissolution, and fractures are all prevalent diagenetic processes. Micritization, cementation, compaction (physical and chemical), dissolution, and dolomitization are among the shallow diagenetic processes (Figure 8) [60–62].

According to the evolution of the environment, these processes display a distinct set of modification conditions. The next section explains the many diagenetic processes that affected the studied carbonates.

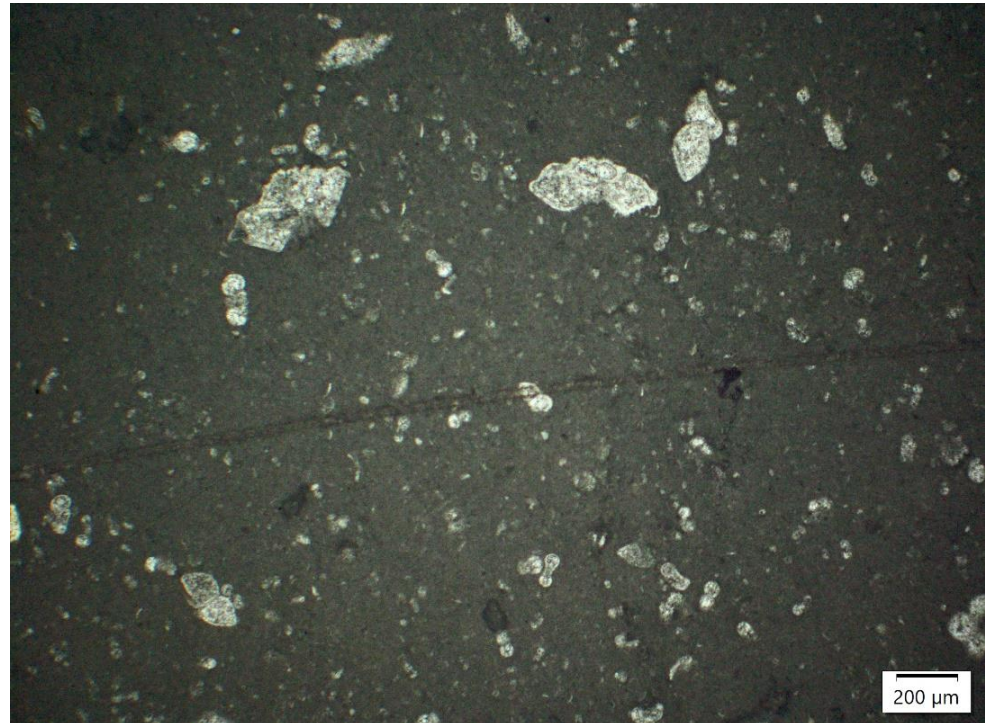


Figure 6. Thin section photomicrograph depicts the co-existence of *Globotruncana stuarti* de Lapparent [56], *Globotruncana aegyptiaca* Nakkady [57], and Globigerinidae determining the K-Pg boundary.

4.4.1. Micritization

The micrite envelopes provide evidence of simultaneous alteration and deposition [63–66]. In general, the micritized skeletal components survive disintegration and act as a surface for late precipitation (Figure 8a). Micrite envelopes are present in all portions of the investigated carbonate samples. The presence of bioclasts in the examined samples indicates a high level of microbial micritization (Figure 8a,b,d). Figure 7a,d show that a micrite envelope covers the grains in the early stages of micritization, whereas other grains have an uneven internal structure and calcite cement filling (Figure 8a). Allochems may be protected from further deterioration by micritization, which has no direct impact on reservoir quality.

4.4.2. Cementation

According to sedimentological features, multiple generations of calcite cement were observed with a modest input of dolomite. The predominant cement type seen was equant calcite spar, which filled interstitial pore spaces, skeletal chambers, and certain pore types (Figure 8b,e,f). In the observation of the epitaxial overgrowth cement (Figure 8e), it is crucial to remark that in certain samples, the overgrowth reaches a length of up to 100 microns. Calcites ranging in size from silty to fine crystalline equants that partly or fully filled fractures (Figure 8c). Additionally, porous, small to medium crystalline, and euhedral dolomite cement fill pore spaces and fractures to a significant extent (Figure 8c,d).

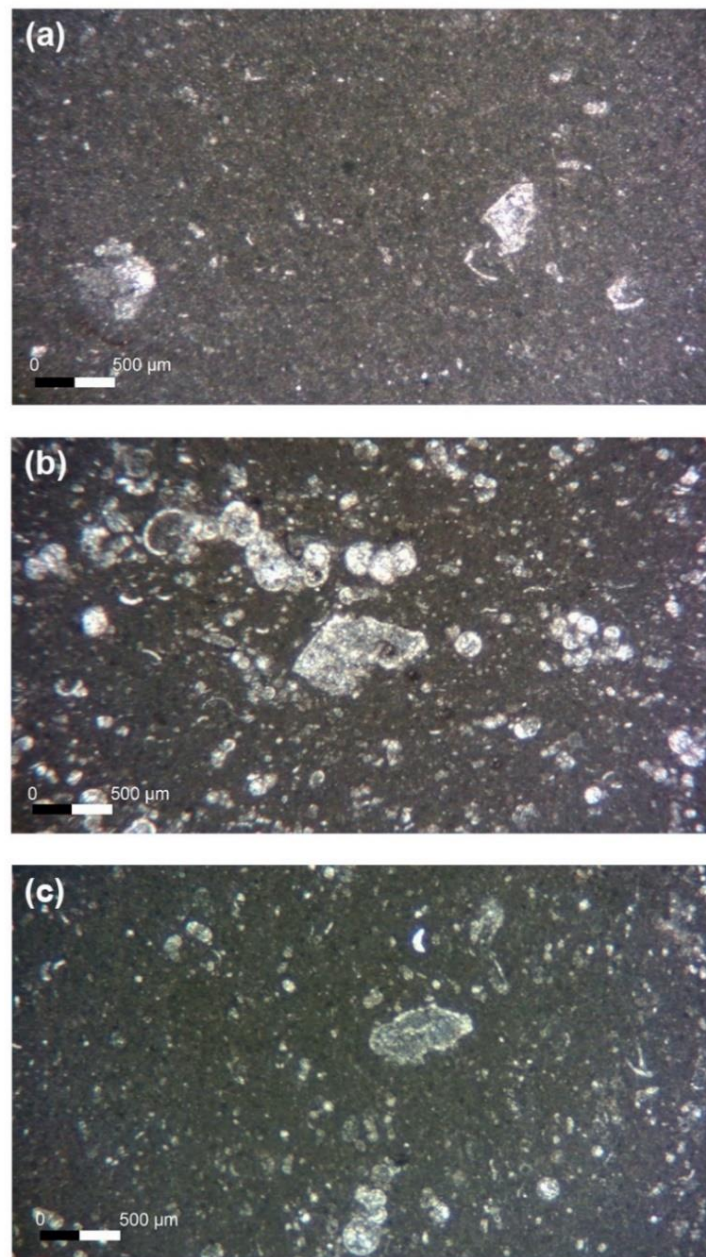


Figure 7. Main microfacies types recognized: (a) Pelagic biomicrite mudstone with planktonic foraminifera, radiolarians, and filaments, (b) Pelagic wackestone–packstone with in situ planktonic foraminifera, (c) Pelagic biomicrite wackestone with altered planktonic foraminifera and/or radiolarians.

4.4.3. Dissolution

Dissolution has been defined as the leaching of metastable bioclasts due to the presence of meteoric water by Budd [67], Morse and Arvidson [68], Lambert et al. [69], Tucker and Wright [70], and Janjuhah et al. [71]. The study rocks are characterized by secondary pore spaces, such as moldic and vuggy pores, developed by dissolution. High-magnesium calcite (HMC) replaces aragonite in the process of dissolution because of the minerals' solubility [72,73]. They also show the most fabric-selective dissolving, with a little proportion originating from non-fabric dissolution (Figure 8a,b,e,f). Late-stage porosity development is indicated by the dissolution that is often seen (Figure 8a,b,e,f). Moldy, vuggy, and fractured porosity are all associated with dissolution (Figure 8a,b,d–f).

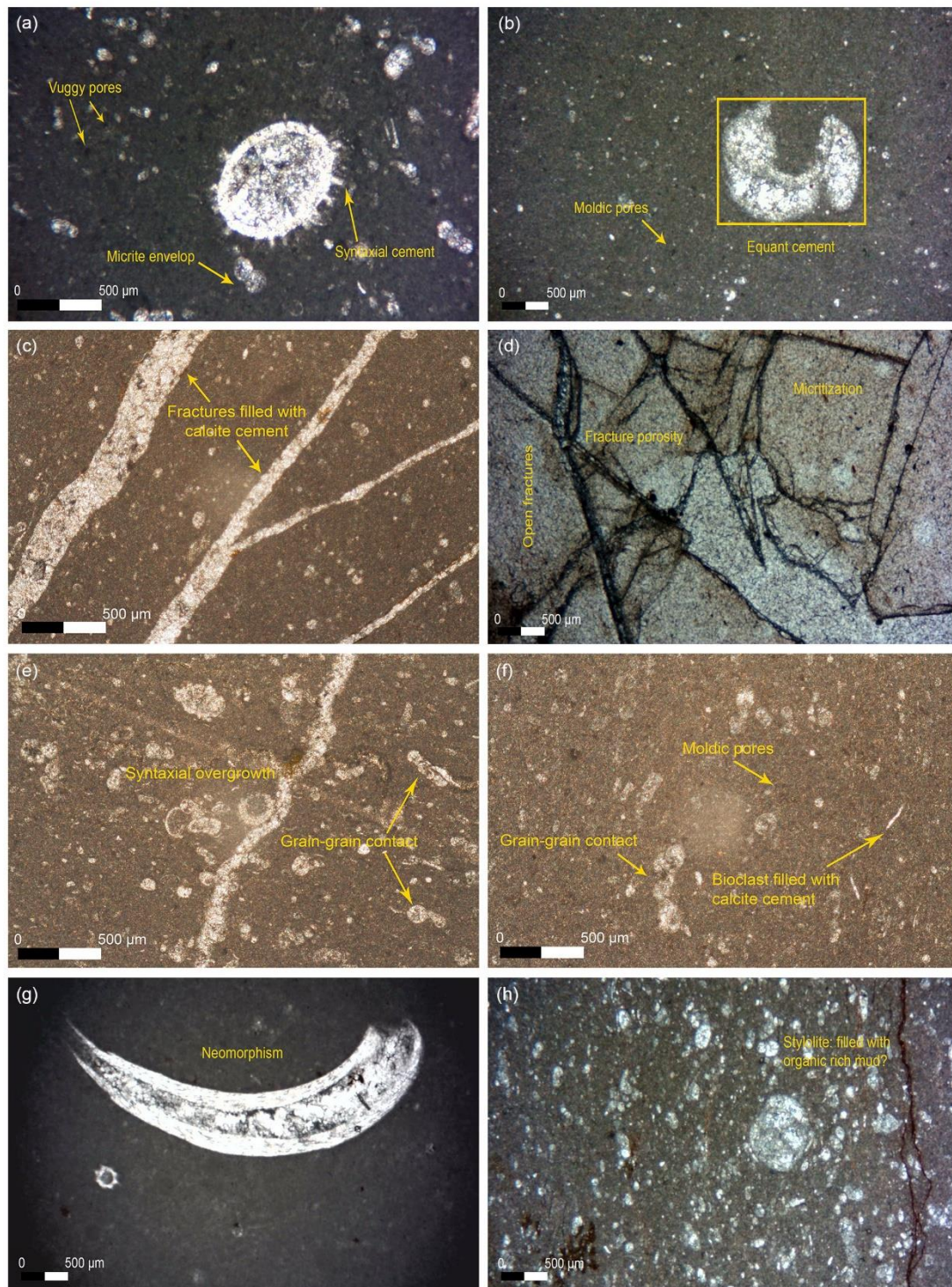


Figure 8. Petrographic analysis showing the different diagenetic processes in carbonate samples collected from Gardiki section (Epirus, Western Greece), (a) high micritization, vuggy pores, and syntactical overgrowth cement, (b) micritization, junctions equant spars of marine moldic pores, (c) micritization, late stage of diagenesis-fractured filled with calcite cement, (d) early stage of micrite envelop, late stage of open fracture, (e) epitaxial overgrowth cement, moldic pores, (f) moldic pores, grain-grain contact (physical compaction), (g) coarse pale brown neomorphic spar replacement of aragonite shell, (h) and stylolites filled with organic-rich mud.

4.4.4. Fracturing

Reservoir quality has improved dramatically due to repeated tectonic stress releases throughout time. Using thin sections, the effectiveness, orientations, and cross-cutting relationships of carbonate fractures can be examined. Their widths vary from a few micrometers to a few centimeters, and their orientations shift from vertical to horizontal. Vertical to sub-vertical fractures dominate the early set, and each fracture is either partly or completely calcite-cement-filled (Figure 8c,d). In contrast, horizontal to sub-horizontal fractures cross-cut the earlier set in the late set. Most of them lack cementation, which improves the reservoirs' quality (Figure 8c,d). Fractures occurred in the burial environment because dissolution seams were generally earlier than the time of formation of the fractures.

4.4.5. Neomorphism

Diagenesis begins immediately upon deposition and continues at all levels until metamorphism takes over. Burial may also be expressed in terms of temperature, pressure, and fluid composition, as well as physical and chemical changes, such as neomorphism. Certain carbonate samples exhibit neomorphism, as seen by the replacement of lime mudstone with finer crystalline calcite spars and the substitution of low magnesium calcite (LMC) for aragonite or high magnesium calcite (HMC) in shell fragments, altering the original texture and structure (Figure 8a,g). Recrystallization of the skeletal particles, either partially or completely, results in aggradation neomorphism (Figure 8g). This process is aided by the presence of calcite with a high magnesium content, which most likely accumulates in the shells of skeletal components until they reach their stable phase under meteorological circumstances [74]. This investigation demonstrated subaerial diagenesis, since numerous skeletal grains have micrite envelopes and exhibit evidence of aggradation neomorphism (Figure 8a).

4.4.6. Compaction

Grain fracture and porosity are reduced because of compaction. Compaction may be caused by mechanical stress, but the chemical reactions are highly dependent on temperature, pressure, and water concentration in the pore space [75]. Compaction may decrease porosity by more than 40% in certain circumstances and is more effective than cementation in reducing porosity [5,76]. The Gardiki carbonates have been affected by both mechanical and chemical compactions. The sediment overburden caused concave–convex grain interactions, which resulted in grain form distortion and breakage (Figure 8e,f).

5. Discussion

5.1. Depositional Conditions and Paleoenvironmental Implications during the K-Pg Transition

The described sedimentary facies distribution reflects a relatively deep environment with some internal differentiations in terms of the environmental deposition and energy conditions (Figure 9). In the Gardiki section of Epirus area, the Senonian post-rift sequence of Ionian basin contains the pelagic biomicrite mudstone (SMF 1-3), whose deposition characterizes a low-energy, deep, basinal environment (FZ1). Even though radiolarians were rarer compared to the planktonic foraminifera in these deposits, the presence of small-sized filaments within the micritic matrix also denotes a relatively deep, low-energy environment. The passage from mixed carbonate-silicious (alterations of limestones and cherts) to almost carbonate material (thin-bedded limestones with sparsely observed siliceous horizons or nodules) during the latest Maastrichtian is indicative of slightly shallower depositional environments close enough to the carbonate compensation depth, such as those of the deep shelf (FZ2). Biomicrite wackestone–packstone with abundant planktonic foraminifera (Globoruncaniids and Globigeriniids; SMF 2-3) characterizes the deposits across the K-Pg boundary. The Early Paleocene massive limestones include in situ bioclastic packstone enriched mostly on planktonic foraminifera (both in situ and reworked) or radiolarians (SMF 3). The micritized nature of the radiolarians (SMF10), where evident, along with some broken foraminifera (SMF 4), indicates a medium-energy environment, possibly

due to their transportation to the basin margin. Such carbonate systems can be usually accumulated in relatively deep parts of the basin, such as the toe of the slope (FZ3-4), and can be further shed from shelf margins.

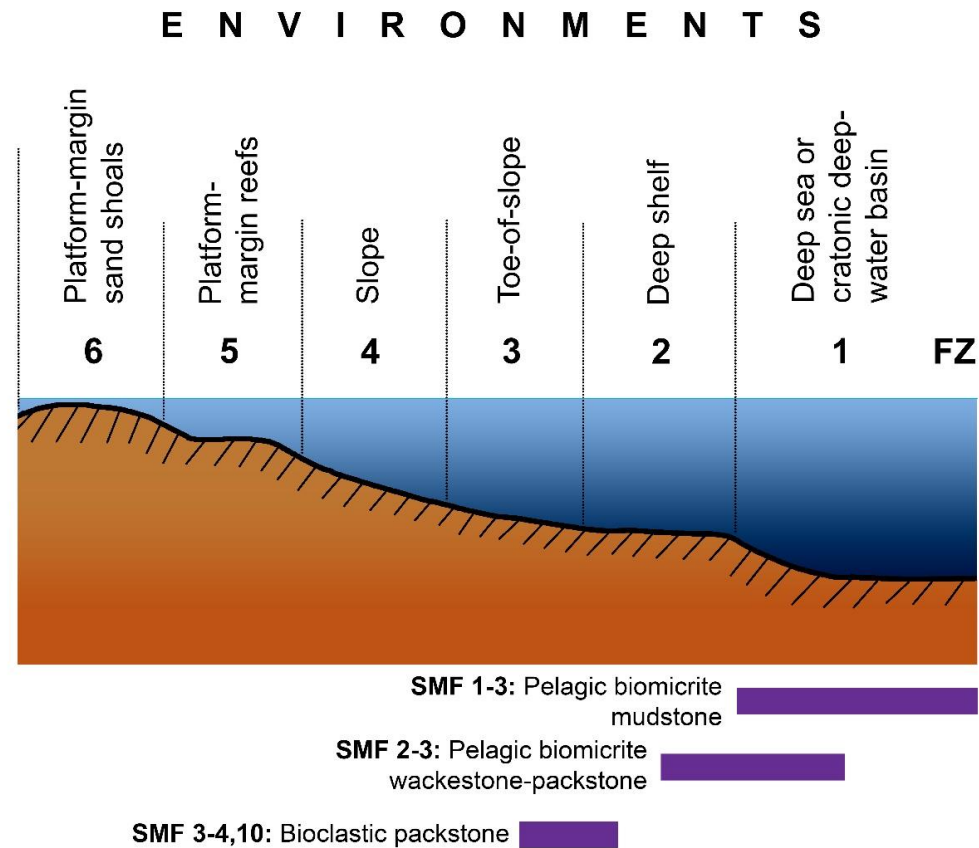


Figure 9. Depositional distribution model for Gardiki section based on microfacies analysis.

Overall, the main depositional facies observed were characterized by pelagic biomicrite mudstone with some planktonic foraminifera, radiolarians, and/or filaments at the base (latest Maastrichtian), packstone with abundant planktonic foraminifera at the middle, and wackestone up to the top of the succession (early Paleocene), implying that the depositional environments across the K-Pg transition did not change significantly. Only a gradual environmental shallowing from the deep basin to the slope can be inferred by the sedimentary facies' interpretation. On the contrary, the transition from the lower to the upper stratigraphically deposits in the study area documents a significant diversification reflected by quite different faunal assemblages, in terms of both their content and abundance. A gradual decrease of in situ radiolarians and increase of planktonic foraminiferal abundance was observed through the Late Cretaceous period, while an abrupt extinction of planktonic foraminifera and the presence of micritized radiolarians were evident at the first samples examined just above the K-Pg boundary (interpreted as a reduction of primary productivity). This kind of differentiation in the fauna was further followed by the subsequent reworking of Globotrunciids (Cretaceous species), as evidenced by broken and aberrant, smaller specimens. Similar abnormal variations in morphology and size of planktonic foraminiferal tests have long been reported globally during the late Maastrichtian crisis [77–79] or immediately above the K-Pg boundary [80–82], and can be compared with similar records documented during other extreme geological events (e.g., Cretaceous ocean anoxic events [83–85]; Paleocene-Eocene Thermal Maximum [86]; Messinian Salinity Crisis [87–89]; Late Pliocene [90]; Sapropel S1 [91]), and seem to reflect mainly stressful environmental conditions in response to changes in ecological parameters (i.e., temperature, salinity, dissolved oxygen, acidification, changeable connectivity; [91–93]) or rapid environ-

mental perturbations (i.e., extreme fluctuations in climate and sea level, intense volcanism, meteoric pollution) [78,82]. As evidenced globally in all extinction events through the Earth history, their duration and the corresponding differences in extinction percentages of foraminiferal taxa inhabiting different levels in the oceanic water column during extinction time intervals are associated with specific environmental parameters, which in turn reveal the causes of these events [94–96]. Particularly for the Cretaceous–Tertiary (K-T) turnover, the most plausible scenario seems to be the alternating climate (global warming during the latest Maastrichtian and Deccan-volcanism induced cooling) and subsequent sea level fluctuations (sea level rise during warming and sea level fall during cooling events), as well as productivity changes [95–97], during which the planktonic foraminiferal species experienced high stress and, in response, reduced their sizes and/or developed malformations on their tests [98,99]. However, besides these key environmental perturbations, additional ecological stress factors could be sufficient to account for the increase of aberrant forms; in some cases, this could even be characterized as lethal for planktonic foraminifera likely contributed to the K-T boundary mass extinction. For instance, the increased concentrations of toxins produced by phytoplankton blooms [100] in surface waters could possibly be related to the proliferations of abnormal planktonic foraminiferal tests above the K-Pg boundary [101,102]. Although such geographically heterogeneous spikes of phytoplankton groups have been reported in the earliest Danian [103], more studies need to establish the above cause–effect relationship. Overall, the observed aberrant forms can be characterized as likely “victims” of the K-T event, highlighting the gradual or sudden foraminiferal extinctions and the related evolutionary and/or ecological crises occurred globally during that time [78,92,104,105].

Particularly for the K-T event, the largest event during the last 100 M.y. [106] is controversial regarding the character (sudden versus gradual) and severity (proportion of surviving species). The biotic turnovers of this mass extinction were highly variable among different fossil groups. Planktic foraminifera were the “losers”, with all tropical and subtropical species (2/3 of all species) extinct, while a few survivors died out during the first 200–300 ky of the Danian [78,81]. Additional quantitative calculations on the decline of diversity of planktonic foraminifera based on the probabilistic stratigraphy technique showed that only a maximum of 22% of Cretaceous species survived the boundary, and 11% passed into the planktonic foraminiferal zone P1a [107]. On the contrary, although calcareous nannoplankton similarly suffered strong declines, several species thrived into the Tertiary, and all other microfossil groups (i.e., dinocysts, benthic foraminifera) reveal minor biotic effects linked with temporal decreases of their diversity and abundance [59,108–112]. The differential planktonic–benthic extinction rate is further supported by the vertical marine carbon isotope gradients ($\Delta\delta^{13}\text{C}$) between planktic and benthic species [113]. Our data exhibit that plankton productivity declined significantly at the K/T boundary, which is consistent with previous studies in a global context, indicating that low productivity levels were more severe in the low latitudes and lasted for a few hundred thousand years before the restoration of normal ecosystems [114–116] through the final recovery of the marine carbon cycle [113,117]. These data may indicate that reduced primary productivity in the surface waters was a main cause of this event, with subsequent reduction in food supply for animals at higher trophic levels [118]. Typically, this low productivity state continued for several hundred thousand years and was associated with widespread stunting of marine organisms (Lilliput effect) and low-biomass ecosystems [95,98,119,120].

At that time in the broad external Ionian zone, allochthonous carbonates were transported to the outer shelf by turbidity currents (calciturbidites) formed by the gravitational collapse of the platform margin [19,20,24]. In the study section, no coarser brecciated horizons were observed within these deposits, as usually happened within the Ionian basin in other locations of the western Greece [19,24,44]. Their absence from the studied part of the Gardiki section could be attributed to the foreland basin evolution, as it was less influenced by their greater distance from the thrusts between the tectonic zones, sediment thickness, and overall depositional conditions. It is most likely that the submarine shelves characterized

the nearby Apulian carbonate platform margins in this setting were not so steep and the instability was not so intense to lead to significant erosion. The smoother slope could provide evidence of slightly eroded platforms internally to the Ionian Basin, thus supporting the half-graben Late Cretaceous concept described in detail by Karakitsios [22]. Overall, this study provides evidence that the supply of clastic material was significantly reduced in this setting during that time, also supporting the findings of Bourli et al. [19] about a differential tectonic activity in the geographic area between Epirus and Kefalonia Island. On the contrary, the deposition of the overlying microbreccious limestones during the Paleocene-Eocene shows that intense debris flow formed by the slumping of the platform margin, possibly due to tectonics, and redeposited the platform edge sediments in the deeper parts of the basin. Consequently, the study deposits reflect the pelagic carbonates that pass into the Eocene calciturbidites.

5.2. Diagenetic History—Paragenesis

Following an investigation of sedimentological relations, we can ascertain the sequence in which diagenetic events took place. The diagenetic history of carbonate rocks in Gardiki section is complex. The K-Pg reservoir deposits of the Ionian zone are divided into three types: marine, meteoric, and burial diagenetic environments (Figure 10).















Samples	Diagenetic Processes	Marine	Meteoric	Burial	Effect on Porosity
B1-B7, B9, B14, B15, B17-B19, B23, B25-B39, B42, B44, B48-B53, B58-B63, B65, B69-B81	Micritization				+ —
B3, B11, B78	Dolomitization				
B1, B3, B15, B17, B18, B19, B42, B44, B65, B69	Fracturing				—
B1-B7, B9, B11, B14-B19, B23, B25-B39, B42, B48-B53, B58-B63, B65, B69-B81	Dissolution (Fabric Selective)				
B1-B7, B9, B11, B14, B15, B17-B19, B23, B25-B38, B42, B48-B53, B58-B63, B65, B69-B81	Cementation				—
	1. Syntaxial cement				
	2. Equant Cement				
B1-B6, B9, B11, B14, B15, B17-B19, B23, B25-B39, B42, B48-B53, B58-B63, B65, B69-B81	3. Blocky Cement				—
	Compaction				
	1. Physical				—
	2. Chemical				
B3, B5, B6, B11, B14, B15, B17, B18, B19, B23, B25-B39, B42, B48-B53, B58-B63, B65, B69-B81	Dissolution (Non-Fabric)				—
B5, B6, B7, B9, B11, B17, B26, B28, B29, B32, B33, B35, B38, B39, B42, B50, B58, B60, B63, B65, B69, B73, B75	Neomorphism				
B1, B3, B4, B7, B9, B11, B15, B17, B23, B25, B27, B32, B34, B35, B42, B52, B60, B62, B65, B69, B76	Filled Fracture and Veins Filling				—

Figure 10. The diagenetic history of K-Pg deposits of Gardiki section based on petrographic observations. Red boxes indicate a strong effect on porosity, and green boxes indicate a low effect on porosity.

5.2.1. Marine Diagenetic Environment

The diagenetic environment of the Late Cretaceous–Early Paleocene reservoir sediments of the Ionian basin (Epirus, western Greece) was in deep basin to shelf deposits. Micritization is quite prevalent during the early stages of diagenesis (Figure 10). During the first stages of micritization, referred to as micritic envelopes, the skeletal grains' surrounding regions were destroyed (Figure 8a,b,d, and Figure 10). This occurs when microboring organisms destroy allochems at or near the sediment–water interface. Brett and Brookfield [121] defined syn-sedimentary micritization as the presence of micritic bioerosion fringes extending from the grain's surface to the grain's core. A marine low-energy environment seems to be favorable for grain micritization and the formation of micritic envelopes around bioclasts in certain samples (Figure 8a,b,d). Additionally, Adams [122]

noted that micritization is the first diagenetic phase that occurs at the sediment–water interface in low-energy shallow marine environments with slow sedimentation rates. According to Karakitsios et al. [123], seawater served as the primary diagnostic fluid in the Ionian basin, resulting in positive/extremely high $\delta^{13}\text{C}$ values for calcites in pores. In the deep slope setting, the early sediment underwent penecontemporaneous and seepage–reflex dolomitization, producing microcrystalline dolomites. Physical compaction, calcite cementation, and dolomitization of the Late Cretaceous reservoir rocks resulted in a considerable reduction of primary porosity (Figure 8a,b,d,e).

5.2.2. Meteoric Diagenetic Environment

The rifting phase occurred during the Late Jurassic–Early Cretaceous period, and the Vigla limestone formation was deposited in the Ionian basin shortly after the rifting phase [34]. Cretaceous strata in western Greece were considerably changed during the Late Cretaceous epoch [124]. As a consequence, during the Late Cretaceous, a meteoric water diagenetic environment may have formed in connection with the global sea-level fall [125,126] $\delta^{13}\text{C}$ value for crystalline limestone is negative, which suggests that recrystallization may also be linked to meteoric freshwater as reported by Tsikos et al. [127].

Meanwhile, dissolution was detected in the rocks examined (Figure 8). Aragonitic organisms, such as bioclasts, had their internal structure partly or entirely disintegrated (Figure 8d). Aragonite's early dissolution might have happened in saltwater or under conditions of shallow burial [128,129]. Two distinct phases of dissolution have been identified. Stage 1 is characterized by the breakdown of aragonitic biota (Figure 8d), implying partial to total bioclast dissolution (HMC grains). Janjuhah et al. [130] noted that meteoric interfaces such as a subaerial exposed surface and the water table are probable locations for significant CO_2 inflow, resulting in enhanced HMC grain dissolving and preventing LMC grain dissolution. Stage 2 is a non-fabric selective matrix dissolution, and a critical diagenetic process in the formation of the study limestones (Figure 8a). Non-fabric selective dissolution occurred between a deep meteoric and a deep burial environment. Following that, the void areas were filled with cement (syntextual, equant, and blocky cement) (Figure 8). They often occur during the same diagenetic period but on distinct substrata. The syntaxial overgrowth cement is often used to enclose bioclast fragments in packstone textures (Figure 8e), while the equant calcite cement is used in both fabric- and non-fabric-selective dissolution (Figure 8c). It is possible to observe equant calcite cement filling the fracture component of the pore spaces between grains (Figure 8c). This cement may be the result of precipitation in a shallow diagenetic environment. Additionally, Flügel [131] reported that equant calcite cement is present in meteoric and burial contexts. It should be noted at this stage that further evidence is required to ascertain if this cement is meteoric- or burial-derived.

5.2.3. Burial Diagenetic Environment

Other diagenetic processes observed in the examined samples include physical and chemical compactions. Physical compaction is defined by rearranged and broken grains that are compressed vertically. Due to early marine cementation and overburden pressure, certain open fractures of mechanical compaction are readily evident (Figure 8d). Chemical compaction is characterized by the formation of a pressure solution of grains and sediments, which serves as an important source of calcium carbonate for burial cementation. The chemical composition of lime mud was identified, which resulted in the invention of stylolites (Figure 8h). The stylolites detected have a relatively small amplitude. Late-stage neomorphism has occurred, affecting the rock. Neomorphism has completely altered the texture and structure of carbonate rocks in the late stage, post-dating early cementation. This process is promoted by the early decomposition of aragonite and HMC in seawater or under very shallow burial circumstances [62]. The most recent diagenetic event was characterized by fractures that crossed other diagenetic products, including the prior

cement and neomorphosed calcite cement (Figure 8e). Later phases, with deep burial (telogenesis), fracturing, and blocky cementation vein filling, occurred [132].

6. Conclusions

An integrated sedimentological analysis of the K-Pg carbonate succession representing the topmost part of the Senonian limestone and the lower part of the microbreccious limestone formation in Gardiki section of Epirus (western Greece) provides new insights into the depositional environment and diagenetic history of the Western Ionian Basin, as well as the synthetic paleoenvironmental reconstruction of the area. The biostratigraphic analysis based on planktonic foraminifera showed that the study interval of the Gardiki section covers the boundary between Late Cretaceous (Maastrichtian) and Paleocene (Danian) time span based on the coexistence of *Globotruncana* spp. and Globigerinidae. Lithostratigraphically, the Senonian limestone formation in this area is mainly characterized by light-grey-to-yellowish limestones, with some siliceous intervals to occur as thin reddish-to-brownish chert intercalations and/or lenses within the pelagic limestone unit. Their presence of both nodular and bedded siliceous concretions is of crucial importance on enhancing the reservoir properties (i.e., secondary porosity and permeability increase) of the hosted deposits through the fracturing and stylolites created during the nodule's development and reveals the potentiality to act as open pathways for the fluids (even for hydrocarbons). The main depositional facies (pelagic biomicrite mudstone to packstone) observed into the K-Pg transition are indicative of a low-energy, basinal to toe-of-slope environmental sedimentation. Minor internal differentiation among them implies that the depositional environment across the K-Pg transition did not change significantly in the external Ionian basin. However, significant differences documented in the content and the abundance of the faunal assemblages testify to the stressful environmental conditions in terms of primary productivity decline that prevailed at that time. Furthermore, the petrographic analysis identified several distinct diagenetic features among the study pelagic carbonates, which are categorized into marine, meteoric, and burial diagenetic settings. Micrite envelop, cementation, fracture, compaction, and dissolution are the dominant diagenetic parameters identified in the study samples, attributing both positive and negative effects on porosity. Overall, this study provides a basis for the further evaluation of the hydrocarbon potential in western continental Greece, which contains proven reserves and is of crucial economic and strategic importance.

Author Contributions: Conceptualization, L.M. and G.K.; methodology, L.M., G.K. and H.T.J.; software, L.M., G.K., H.T.J. and A.Z.-L.; validation, L.M., G.K., H.T.J. and A.Z.-L.; formal analysis, L.M., G.K., H.T.J., A.Z.-L.; investigation, L.M., G.K., H.T.J., A.Z.-L., D.G., P.P., C.K., S.S., E.B., V.K. and A.A.; resources, L.M., G.K., V.K.; data curation, L.M., G.K., H.T.J., A.Z.-L. and C.K.; writing—original draft preparation, L.M., G.K. and H.T.J.; writing—review and editing, L.M., G.K., H.T.J., A.Z.-L., D.G., P.P., C.K., S.S., E.B., V.K. and A.A.; visualization, L.M. and G.K.; supervision, A.A. and V.K.; project administration, G.K., A.A.; funding acquisition, G.K. All authors have read and agreed to the published version of the manuscript.

Funding: This research received no external funding.

Institutional Review Board Statement: Not applicable.

Informed Consent Statement: Not applicable.

Data Availability Statement: The data used in this work is available on request to the corresponding authors.

Conflicts of Interest: The authors declare no conflict of interest.

References

1. Knowlton, N.; Brainard, R.E.; Fisher, R.; Moews, M.; Plaisance, L.; Caley, M.J. Coral Reef Biodiversity. In *Life in the World's Oceans*; John Wiley & Sons: Hoboken, NJ, USA, 2010; pp. 65–78. [\[CrossRef\]](#)
2. Falkowski, P.; Scholes, R.J.; Boyle, E.; Canadell, J.; Canfield, D.; Elser, J.; Gruber, N.; Hibbard, K.; Höglberg, P.; Linder, S.; et al. The Global Carbon Cycle: A Test of Our Knowledge of Earth as a System. *Science* **2000**, *290*, 291–296. [\[CrossRef\]](#) [\[PubMed\]](#)

3. Burchette Trevor, P. Carbonate rocks and petroleum reservoirs: A geological perspective from the industry. *Geol. Soc. Lond. Spec. Publ.* **2012**, *370*, 17–37. [\[CrossRef\]](#)
4. Ahmad, I.; Shah, M.M.; Janjuhah, H.T.; Trave, A.; Antonarakou, A.; Kontakiotis, G. Multiphase Diagenetic Processes and Their Impact on Reservoir Character of the Late Triassic (Rhaetian) Kingriali Formation, Upper Indus Basin, Pakistan. *Minerals* **2022**, *12*, 1049. [\[CrossRef\]](#)
5. Janjuhah, H.T.; Kontakiotis, G.; Wahid, A.; Khan, D.M.; Zarkogiannis, S.D.; Antonarakou, A. Integrated Porosity Classification and Quantification Scheme for Enhanced Carbonate Reservoir Quality: Implications from the Miocene Malaysian Carbonates. *J. Mar. Sci. Eng.* **2021**, *9*, 1410. [\[CrossRef\]](#)
6. Laugié, M.; Michel, J.; Pohl, A.; Poli, E.; Borgomano, J. Global distribution of modern shallow-water marine carbonate factories: A spatial model based on environmental parameters. *Sci. Rep.* **2019**, *9*, 16432. [\[CrossRef\]](#)
7. Michel, J.; Laugié, M.; Pohl, A.; Lanteaume, C.; Masse, J.-P.; Donnadieu, Y.; Borgomano, J. Marine carbonate factories: A global model of carbonate platform distribution. *Int. J. Earth Sci.* **2019**, *108*, 1773–1792. [\[CrossRef\]](#)
8. Kontakiotis, G.; Karakitsios, V.; Mortyn, P.G.; Antonarakou, A.; Drinia, H.; Anastasakis, G.; Agiadi, K.; Kafousia, N.; De Rafelis, M. New insights into the early Pliocene hydrographic dynamics and their relationship to the climatic evolution of the Mediterranean Sea. *Palaeogeogr. Palaeoclimatol. Palaeoecol.* **2016**, *459*, 348–364. [\[CrossRef\]](#)
9. Kontakiotis, G.; Besiou, E.; Antonarakou, A.; Zarkogiannis, S.D.; Kostis, A.; Mortyn, P.G.; Moissette, P.; Cornée, J.J.; Schulbert, C.; Drinia, H.; et al. Decoding sea surface and paleoclimate conditions in the eastern Mediterranean over the Tortonian-Messinian Transition. *Palaeogeogr. Palaeoclimatol. Palaeoecol.* **2019**, *534*, 109312. [\[CrossRef\]](#)
10. Kontakiotis, G.; Butiseacă, G.A.; Antonarakou, A.; Agiadi, K.; Zarkogiannis, S.D.; Krsnik, E.; Besiou, E.; Zachariasse, W.J.; Lourens, L.; Thivaoui, D.; et al. Hypersalinity accompanies tectonic restriction in the eastern Mediterranean prior to the Messinian Salinity Crisis. *Palaeogeogr. Palaeoclimatol. Palaeoecol.* **2022**, *592*, 110903. [\[CrossRef\]](#)
11. Goldscheider, N.; Mádl-Szőnyi, J.; Erőss, A.; Schill, E. Review: Thermal water resources in carbonate rock aquifers. *Hydrogeol. J.* **2010**, *18*, 1303–1318. [\[CrossRef\]](#)
12. Kiessling, W.; Flügel, E.; Golonka, J.A.N. Patterns of Phanerozoic carbonate platform sedimentation. *Lethaia* **2003**, *36*, 195–225. [\[CrossRef\]](#)
13. Pohl, A.; Laugié, M.; Borgomano, J.; Michel, J.; Lanteaume, C.; Scotese, C.R.; Frau, C.; Poli, E.; Donnadieu, Y. Quantifying the paleogeographic driver of Cretaceous carbonate platform development using paleoecological niche modeling. *Palaeogeogr. Palaeoclimatol. Palaeoecol.* **2019**, *514*, 222–232. [\[CrossRef\]](#)
14. Philip, J.; Masse, J.-P.; Camoin, G. Tethyan Carbonate Platforms. In *The Tethys Ocean*; Nairn, A.E.M., Ricou, L.-E., Vrielynck, B., Dercourt, J., Eds.; Springer: Boston, MA, USA, 1996; pp. 239–265. [\[CrossRef\]](#)
15. Bernoulli, D.; Jenkyns, H.C. Alpine, Mediterranean, and Central Atlantic Mesozoic Facies in Relation to the Early Evolution of the Tethys. In *Modern and Ancient Geosynclinal Sedimentation*; Dott, R.H., Jr., Shaver, R.H., Eds.; SEPM Society for Sedimentary Geology: Tulsa, OK, USA, 1974; Volume 19. [\[CrossRef\]](#)
16. Belghouthi, F. The Upper Cretaceous-Lower Eocene carbonate platforms of the Mateur-Beja area (NW of Tunisia): A pattern of isolated platform. *J. Afr. Earth Sci.* **2022**, *187*, 104453. [\[CrossRef\]](#)
17. Jurkowska, A.; Świerczewska-Gładysz, E.; Bąk, M.; Kowalik, S. The role of biogenic silica in the formation of Upper Cretaceous pelagic carbonates and its palaeoecological implications. *Cretac. Res.* **2019**, *93*, 170–187. [\[CrossRef\]](#)
18. Bourli, N.; Kokkaliari, M.; Iliopoulos, I.; Pe-Piper, G.; Piper, D.J.W.; Maravelis, A.G.; Zelilidis, A. Mineralogy of siliceous concretions, cretaceous of ionian zone, western Greece: Implication for diagenesis and porosity. *Mar. Pet. Geol.* **2019**, *105*, 45–63. [\[CrossRef\]](#)
19. Bourli, N.; Pantopoulos, G.; Maravelis, A.G.; Zoumpoulis, E.; Iliopoulos, G.; Pomoni-Papaioannou, F.; Kostopoulou, S.; Zelilidis, A. Late Cretaceous to early Eocene geological history of the eastern Ionian Basin, southwestern Greece: A sedimentological approach. *Cretac. Res.* **2019**, *98*, 47–71. [\[CrossRef\]](#)
20. Kontakiotis, G.; Moforis, L.; Karakitsios, V.; Antonarakou, A. Sedimentary Facies Analysis, Reservoir Characteristics and Paleogeography Significance of the Early Jurassic to Eocene Carbonates in Epirus (Ionian Zone, Western Greece). *J. Mar. Sci. Eng.* **2020**, *8*, 706. [\[CrossRef\]](#)
21. Karakitsios, V.; Rigakis, N. Evolution and petroleum potential of Western Greece. *J. Pet. Geol.* **2007**, *30*, 197–218. [\[CrossRef\]](#)
22. Karakitsios, V. Western Greece and Ionian petroleum systems. *AAPG Bull.* **2013**, *97*, 1567–1595. [\[CrossRef\]](#)
23. Zelilidis, A.; Maravelis, A.G.; Tserolas, P.; Konstantopoulos, P.A. An overview of the petroleum systems in the Ionian zone, onshore NW Greece and Albania. *J. Pet. Geol.* **2015**, *38*, 331–348. [\[CrossRef\]](#)
24. Zoumpouli, E.; Maravelis, A.G.; Iliopoulos, G.; Botziolis, C.; Zygouri, V.; Zelilidis, A. Re-Evaluation of the Ionian Basin Evolution during the Late Cretaceous to Eocene (Aetoloakarnania Area, Western Greece). *Geosciences* **2022**, *12*, 106. [\[CrossRef\]](#)
25. Tserolas, P.; Maravelis, A.G.; Tsochandar, N.; Pasadakis, N.; Zelilidis, A. Organic geochemistry of the Upper Miocene-Lower Pliocene sedimentary rocks in the Hellenic Fold and Thrust Belt, NW Corfu island, Ionian sea, NW Greece. *Mar. Pet. Geol.* **2019**, *106*, 17–29. [\[CrossRef\]](#)
26. Papanikolaou, D. Tectonostratigraphic models of the Alpine terranes and subduction history of the Hellenides. *Tectonophysics* **2013**, *595–596*, 1–24. [\[CrossRef\]](#)
27. Papanikolaou, D.I. Organization and Evolution of the Tethyan Alpine System. In *The Geology of Greece*; Papanikolaou, D.I., Ed.; Springer International Publishing: Cham, Switzerland, 2021; pp. 9–24. [\[CrossRef\]](#)

28. Aubouin, J.; Le Pichon, X.; Winterer, E.; Bonneau, M. *Les Hellénides dans l'optique de la tectonique des plaques, 6th Colloquium on the Geology of the Aegean Region, Athens, 1977*; Reprinted from proceedings vol. III; IGME: Athens, Greece, 1979; Volume 3, pp. 1333–1354.
29. Papanikolaou, D. The tectonostratigraphic terranes of the Hellenides. *Ann. Geol. Des. Pays Hell.* **1997**, *37*, 495–514.
30. Papanikolaou, D.I. Greece Within the Alpine Orogenic System. In *The Geology of Greece*; Papanikolaou, D.I., Ed.; Springer International Publishing: Cham, Switzerland, 2021; pp. 1–8. [\[CrossRef\]](#)
31. Aubouin, J. Contribution à l'étude géologique de la Grèce septentrionale: Les confins de l'Épire et de la Thessalie; Place des Hellénides parmi les édifices structuraux de la Méditerranée orientale. *Ann. Geol. Des. Pays Hell.* **1959**, *10*, 1–483.
32. IGRS-IFP. *Étude Géologique de l'Épire (Grèce Nord—Occidentale)*; Technip & Ophrys Editions: Paris, France, 1966.
33. Dragastan, O.; Papanikos, D.; Papanikos, P. Foraminifères, Algues et Micrproblematica du Trias de Messopotamos, Épire (Grèce continentale). *Rev. Micropaléontologie* **1985**, *27*, 244–248.
34. Karakitsios, V. Chronologie et Geometrie de L'ouverture d'un Bassin et de son Inversion Tectonique: Le Bassin Ionien (Épire, Grèce). *Mem. Sc. Terre Univ.* **1990**, *6*, 91–94.
35. Karakitsios, V. Ouverture et inversion tectonique du Bassin Ionien (Épire, Grèce). *Ann. Géologiques Des Pays Helléniques* **1992**, *35*, 185–318.
36. Karakitsios, V.; Tsaila-Monopolis, V. Données nouvelles sur les niveaux inférieurs Trias supérieur de la série calcaire ionienne en Épire Grèce continentale Conséquences stratigraphiques. *Rev. Paleobiol.* **1988**, *91*, 139–147.
37. Karakitsios, V. The Influence of Preexisting Structure and Halokinesis on Organic Matter Preservation and Thrust System Evolution in the Ionian Basin, Northwest Greece. *AAPG Bull.* **1995**, *79*, 960–980. [\[CrossRef\]](#)
38. Bernoulli, D.; Renz, O. Jurassic carbonate facies and new ammonite faunas from western Greece. *Eclog. Eclogae Geol. Helv.* **1970**, *63*, 573–607.
39. Karakitsios, V.; Koletti, L. Critical Revision of the Age of the Basal Vigla Limestones (Ionian Zone, Western Greece), Based on Nannoplankton and Calpionellids, with Paleogeographical Consequences. In Proceedings of the 4th International Nannoplankton Association Conference, Prague, Czech Republic, 1 September 1992; pp. 165–177.
40. Skourtsis-Coroneou, V.; Solakius, N.; Constantinidis, I. Cretaceous stratigraphy of the Ionian Zone, Hellenides, western Greece. *Cretac. Res.* **1995**, *16*, 539–558. [\[CrossRef\]](#)
41. Dunham, R.J. *Classification of Carbonate Rocks According to Depositional Textures*; American Association of Petroleum Geologists: Tulsa, OK, USA, 1962.
42. Embry, A.F.; Klován, J.E. A late Devonian reef tract on northeastern Banks Island, NWT. *Bull. Can. Pet. Geol.* **1971**, *19*, 730–781. [\[CrossRef\]](#)
43. Flügel, E. Microfacies analysis of carbonate rocks. In *Analysis, Interpretation and Application*; Springer: Berlin/Heidelberg, Germany, 2004.
44. Bourli, N.; Iliopoulos, G.; Papadopoulou, P.; Zelilidis, A. Microfacies and Depositional Conditions of Jurassic to Eocene Carbonates: Implication on Ionian Basin Evolution. *Geosciences* **2021**, *11*, 288. [\[CrossRef\]](#)
45. Bourli, N.; Kokkaliari, M.; Dimopoulos, N.; Iliopoulos, I.; Zoumpouli, E.; Iliopoulos, G.; Zelilidis, A. Comparison between Siliceous Concretions from the Ionian Basin and the Apulian Platform Margins (Pre-Apulian Zone), Western Greece: Implication of Differential Diagenesis on Nodules Evolution. *Minerals* **2021**, *11*, 890. [\[CrossRef\]](#)
46. Ali, S.K.; Janjuhah, H.T.; Shahzad, S.M.; Kontakiotis, G.; Saleem, M.H.; Khan, U.; Zarkogiannis, S.D.; Makri, P.; Antonarakou, A. Depositional Sedimentary Facies, Stratigraphic Control, Paleogeological Constraints, and Paleogeographic Reconstruction of Late Permian Chhidru Formation (Western Salt Range, Pakistan). *J. Mar. Sci. Eng.* **2021**, *9*, 1372. [\[CrossRef\]](#)
47. Fazal, A.G.; Umar, M.; Shah, F.; Miraj, M.A.; Janjuhah, H.T.; Kontakiotis, G.; Jan, A.K. Geochemical Analysis of Cretaceous Shales from the Hazara Basin, Pakistan: Provenance Signatures and Paleo-Weathering Conditions. *J. Mar. Sci. Eng.* **2022**, *10*, 1654. [\[CrossRef\]](#)
48. Rahim, H.-u.; Qamar, S.; Shah, M.M.; Corbella, M.; Martín-Martín, J.D.; Janjuhah, H.T.; Navarro-Ciurana, D.; Lianou, V.; Kontakiotis, G. Processes Associated with Multiphase Dolomitization and Other Related Diagenetic Events in the Jurassic Samana Suk Formation, Himalayan Foreland Basin, NW Pakistan. *Minerals* **2022**, *12*, 1320. [\[CrossRef\]](#)
49. Zaheer, M.; Khan, M.R.; Mughal, M.S.; Janjuhah, H.T.; Makri, P.; Kontakiotis, G. Petrography and Lithofacies of the Siwalik Group in the Core of Hazara-Kashmir Syntaxis: Implications for Middle Stage Himalayan Orogeny and Paleoclimatic Conditions. *Minerals* **2022**, *12*, 1055. [\[CrossRef\]](#)
50. Bilal, A.; Mughal, M.S.; Janjuhah, H.T.; Ali, J.; Niaz, A.; Kontakiotis, G.; Antonarakou, A.; Usman, M.; Hussain, S.A.; Yang, R. Petrography and Provenance of the Sub-Himalayan Kuldana Formation: Implications for Tectonic Setting and Palaeoclimatic Conditions. *Minerals* **2022**, *12*, 794. [\[CrossRef\]](#)
51. Ruidas, D.K.; Pomoni-Papaioannou, F.A.; Banerjee, S.; Gangopadhyay, T.K. Petrographical and geochemical constraints on carbonate diagenesis in an epeiric platform deposit: Late Cretaceous Bagh Group in central India. *Carbonates Evaporites* **2020**, *35*, 94. [\[CrossRef\]](#)
52. Zambetakis-Lekkas, A.; Pomoni-Papaioannou, F.; Alexopoulos, A. Biostratigraphical and sedimentological study of Upper Senonian–Lower Eocene sediments of Tripolitza Platform in central Crete (Greece). *Cretac. Res.* **1998**, *19*, 715–732. [\[CrossRef\]](#)
53. Bilal, A.; Yang, R.; Mughal, M.S.; Janjuhah, H.T.; Zaheer, M.; Kontakiotis, G. Sedimentology and Diagenesis of the Early–Middle Eocene Carbonate Deposits of the Ceno-Tethys Ocean. *J. Mar. Sci. Eng.* **2022**, *10*, 1794.

54. Bilal, A.; Yang, R.; Fan, A.; Mughal, M.S.; Li, Y.; Basharat, M.; Farooq, M. Petrofacies and diagenesis of Thanetian Lockhart Limestone in the Upper Indus Basin (Pakistan): Implications for the Ceno-Tethys Ocean. *Carbonates Evaporites* **2022**, *37*, 78. [\[CrossRef\]](#)
55. IGME. *Geological Map of Greek Series, Paramythia Sheet, Scale 1:50.000*; Institute for Geology and Subsurface Research: Athens, Greece, 1966.
56. de Lapparent, J. *Etude Lithologique des Terrains Crétacés de la Région d'Hendaye*; Imprimerie Nationale: Paris, France, 1918.
57. Nakkady, S. A new foraminiferal fauna from the Esna shales and upper Cretaceous Chalk of Egypt. *J. Paleontol.* **1950**, *24*, 675–692.
58. Huber, B.T.; MacLeod, K.G.; Norris, R.D. Abrupt extinction and subsequent reworking of Cretaceous planktonic Foraminifera across the Cretaceous-Tertiary boundary: Evidence from the subtropical North Atlantic. In *Catastrophic Events and Mass Extinctions: Impacts and Beyond*; Koeberl, C., MacLeod, K.G., Eds.; Geological Society of America: Boulder, CO, USA, 2002; Volume 356.
59. Beiranvand, B.; Zaghib-Turki, D.; Ghasemi-Nejad, E. Integrated biostratigraphy based on planktonic foraminifera and dinoflagellates across the Cretaceous/Paleogene (K/Pg) transition at the Izeh section (SW Iran). *Comptes Rendus Palevol* **2014**, *13*, 235–258. [\[CrossRef\]](#)
60. Scholle, P.A.; Ulmer-Scholle, D.S. *A Color Guide to the Petrography of Carbonate Rocks: Grains, Textures, Porosity, Diagenesis*; American Association of Petroleum Geologists: Tulsa, OK, USA, 2003. [\[CrossRef\]](#)
61. Janjuhah, H.T.; Alansari, A. Offshore Carbonate Facies Characterization and Reservoir Quality of Miocene Rocks in the Southern Margin of South China Sea. *Acta Geol. Sin.—Engl. Ed.* **2020**, *94*, 1547–1561. [\[CrossRef\]](#)
62. Janjuhah, H.T.; Alansari, A.; Ghosh, D.P.; Bashir, Y. New approach towards the classification of microporosity in Miocene carbonate rocks, Central Luconia, offshore Sarawak, Malaysia. *J. Nat. Gas Geosci.* **2018**, *3*, 119–133. [\[CrossRef\]](#)
63. Tomašových, A.; Gallmetzer, I.; Haselmair, A.; Zuschin, M. Inferring time averaging and hiatus durations in the stratigraphic record of high-frequency depositional sequences. *Sedimentology* **2022**, *69*, 1083–1118. [\[CrossRef\]](#)
64. Sharifi-Yazdi, M.; Rahimpour-Bonab, H.; Tavakoli, V.; Nazemi, M.; Kamali, M.R. Linking diagenetic history to depositional attributes in a high-frequency sequence stratigraphic framework: A case from upper Jurassic Arab formation in the central Persian Gulf. *J. Afr. Earth Sci.* **2019**, *153*, 91–110. [\[CrossRef\]](#)
65. Janjuhah, H.T.; Salim, A.M.A.; Ghosh, D.P.; Wahid, A. Diagenetic Process and Their Effect on Reservoir Quality in Miocene Carbonate Reservoir, Offshore, Sarawak, Malaysia. In Proceedings of the ICIPEG 2016, Singapore, 31 January 2017; pp. 545–558.
66. Janjuhah, H.T.; Salim, A.M.A.; Ghosh, D.P. Sedimentology and reservoir geometry of the Miocene Carbonate deposits in Central Luconia, Offshore, Sarawak, Malaysia. *J. Appl. Sci.* **2017**, *17*, 153–170. [\[CrossRef\]](#)
67. Budd, D.A. The Relative Roles of Compaction and Early Cementation in the Destruction of Permeability in Carbonate Grainstones: A Case Study from the Paleogene of West-Central Florida, U.S.A. *J. Sediment. Res.* **2002**, *72*, 116–128. [\[CrossRef\]](#)
68. Morse, J.W.; Arvidson, R.S. The dissolution kinetics of major sedimentary carbonate minerals. *Earth-Sci. Rev.* **2002**, *58*, 51–84. [\[CrossRef\]](#)
69. Lambert, L.; Durllet, C.; Loreau, J.-P.; Marnier, G. Burial dissolution of micrite in Middle East carbonate reservoirs (Jurassic–Cretaceous): Keys for recognition and timing. *Mar. Pet. Geol.* **2006**, *23*, 79–92. [\[CrossRef\]](#)
70. Tucker, M.E.; Wright, V.P. *Carbonate Sedimentology*; Wiley-Blackwell: New York, NY, USA, 2009; p. 496.
71. Janjuhah, H.T.; GÁmez Vintaned, J.A.; Salim, A.M.A.; Faye, I.; Shah, M.M.; Ghosh, D.P. Microfacies and Depositional Environments of Miocene Isolated Carbonate Platforms from Central Luconia, Offshore Sarawak, Malaysia. *Acta Geol. Sin.—Engl. Ed.* **2017**, *91*, 1778–1796. [\[CrossRef\]](#)
72. Morse, J.W.; Arvidson, R.S.; Lüttge, A. Calcium Carbonate Formation and Dissolution. *Chem. Rev.* **2007**, *107*, 342–381. [\[CrossRef\]](#) [\[PubMed\]](#)
73. Janjuhah, H.T.; Salim, A.M.A.; Shah, M.M.; Ghosh, D.; Alansari, A. Quantitative interpretation of carbonate reservoir rock using wireline logs: A case study from Central Luconia, offshore Sarawak, Malaysia. *Carbonates Evaporites* **2017**, *32*, 591–607. [\[CrossRef\]](#)
74. Amel, H.; Jafarian, A.; Husinec, A.; Koeshidayatullah, A.; Swennen, R. Microfacies, depositional environment and diagenetic evolution controls on the reservoir quality of the Permian Upper Dalan Formation, Kish Gas Field, Zagros Basin. *Mar. Pet. Geol.* **2015**, *67*, 57–71. [\[CrossRef\]](#)
75. Xi, K.; Cao, Y.; Jähren, J.; Zhu, R.; Bjørlykke, K.; Haile, B.G.; Zheng, L.; Hellevang, H. Diagenesis and reservoir quality of the Lower Cretaceous Quantou Formation tight sandstones in the southern Songliao Basin, China. *Sediment. Geol.* **2015**, *330*, 90–107. [\[CrossRef\]](#)
76. Janjuhah, H.T.; Sanjuan, J.; Alqudah, M.; Salah, M.K. Biostratigraphy, Depositional and Diagenetic Processes in Carbonate Rocks from Southern Lebanon: Impact on Porosity and Permeability. *Acta Geol. Sin.—Engl. Ed.* **2021**, *95*, 1668–1683. [\[CrossRef\]](#)
77. Abramovich, S.; Keller, G. High stress late Maastrichtian paleoenvironment: Inference from planktonic foraminifera in Tunisia. *Palaeogeogr. Palaeoclimatol. Palaeoecol.* **2002**, *178*, 145–164. [\[CrossRef\]](#)
78. Keller, G.; Adatte, T.; Tantawy, A.A.; Berner, Z.; Stinnesbeck, W.; Stueben, D.; Leanza, H.A. High stress late Maastrichtian—Early Danian palaeoenvironment in the Neuquén Basin, Argentina. *Cretac. Res.* **2007**, *28*, 939–960. [\[CrossRef\]](#)
79. Omaña, L.; Alencáster, G.; Torres Hernández, J.R.; López Doncel, R. Morphological Abnormalities and Dwarfism in Maastrichtian Foraminifera from the Cárdenas Formation, Valles-San Luis Potosí Platform, Mexico: Evidence of paleoenvironmental stress. *Boletín Soc. Geológica Mex.* **2012**, *64*, 305–318. [\[CrossRef\]](#)
80. Luciani, V. Planktonic foraminiferal turnover across the Cretaceous-Tertiary boundary in the Vajont valley (Southern Alps, northern Italy). *Cretac. Res.* **1997**, *18*, 799–821. [\[CrossRef\]](#)

81. Arenillas, I.; Arz, J.A.; Gilabert, V. Blooms of aberrant planktic foraminifera across the K/Pg boundary in the Western Tethys: Causes and evolutionary implications. *Paleobiology* **2018**, *44*, 460–489. [\[CrossRef\]](#)
82. Coccioni, R.; Luciani, V. Guembelitra irregularis bloom at the KT boundary: Morphological abnormalities induced by impact-related extreme environmental stress? In *Biological Processes Associated with Impact Events*; Springer: Berlin/Heidelberg, Germany, 2006; pp. 179–196.
83. Coccioni, R.; Luciani, V.; Marsili, A. Cretaceous oceanic anoxic events and radially elongated chambered planktonic foraminifera: Paleoeological and paleoceanographic implications. *Palaeogeogr. Palaeoclimatol. Palaeoecol.* **2006**, *235*, 66–92. [\[CrossRef\]](#)
84. Verga, D.; Premoli Silva, I. Early Cretaceous planktonic foraminifera from the Tethys: The genus Leupoldina. *Cretac. Res.* **2002**, *23*, 189–212. [\[CrossRef\]](#)
85. Verga, D.; Premoli Silva, I. Early Cretaceous planktonic foraminifera from the Tethys: The small, few-chambered representatives of the genus Globigerinelloides. *Cretac. Res.* **2003**, *24*, 305–334. [\[CrossRef\]](#)
86. Luciani, V.; Giusberti, L.; Agnini, C.; Backman, J.; Fornaciari, E.; Rio, D. The Paleocene–Eocene Thermal Maximum as recorded by Tethyan planktonic foraminifera in the Forada section (northern Italy). *Mar. Micropaleontol.* **2007**, *64*, 189–214. [\[CrossRef\]](#)
87. Corbí, H.; Soria, J.M.; Lancis, C.; Giannetti, A.; Tent-Manclús, J.E.; Dinarès-Turell, J. Sedimentological and paleoenvironmental scenario before, during, and after the Messinian Salinity Crisis: The San Miguel de Salinas composite section (western Mediterranean). *Mar. Geol.* **2016**, *379*, 246–266. [\[CrossRef\]](#)
88. Vasiliev, I.; Karakitsios, V.; Bouloubassi, I.; Agiadi, K.; Kontakiotis, G.; Antonarakou, A.; Triantaphyllou, M.; Gogou, A.; Kafousia, N.; de Rafélis, M.; et al. Large Sea Surface Temperature, Salinity, and Productivity-Preservation Changes Preceding the Onset of the Messinian Salinity Crisis in the Eastern Mediterranean Sea. *Paleoceanogr. Paleoclimatol.* **2019**, *34*, 182–202. [\[CrossRef\]](#)
89. Karakitsios, V.; Roveri, M.; Lugli, S.; Manzi, V.; Gennari, R.; Antonarakou, A.; Triantaphyllou, M.; Agiadi, K.; Kontakiotis, G.; Kafousia, N.; et al. A record of the Messinian salinity crisis in the eastern Ionian tectonically active domain (Greece, eastern Mediterranean). *Basin Res.* **2017**, *29*, 203–233. [\[CrossRef\]](#)
90. Wade, B.S.; Olsson, R.K. Investigation of pre-extinction dwarfing in Cenozoic planktonic foraminifera. *Palaeogeogr. Palaeoclimatol. Palaeoecol.* **2009**, *284*, 39–46. [\[CrossRef\]](#)
91. Antonarakou, A.; Kontakiotis, G.; Zarkogiannis, S.; Mortyn, P.G.; Drinia, H.; Koskeridou, E.; Anastasakis, G. Planktonic foraminiferal abnormalities in coastal and open marine eastern Mediterranean environments: A natural stress monitoring approach in recent and early Holocene marine systems. *J. Mar. Syst.* **2018**, *181*, 63–78. [\[CrossRef\]](#)
92. Pardo, A.; Keller, G. Biotic effects of environmental catastrophes at the end of the Cretaceous and early Tertiary: Guembelitra and Heterohelix blooms. *Cretac. Res.* **2008**, *29*, 1058–1073. [\[CrossRef\]](#)
93. Agiadi, K.; Antonarakou, A.; Kontakiotis, G.; Kafousia, N.; Moissette, P.; Cornée, J.-J.; Manoutsoglou, E.; Karakitsios, V. Connectivity controls on the late Miocene eastern Mediterranean fish fauna. *Int. J. Earth Sci.* **2017**, *106*, 1147–1159. [\[CrossRef\]](#)
94. Kaiho, K. Planktonic and benthic foraminiferal extinction events during the last 100 m.y. *Palaeogeogr. Palaeoclimatol. Palaeoecol.* **1994**, *111*, 45–71. [\[CrossRef\]](#)
95. Twitchett, R.J. The palaeoclimatology, palaeoecology and palaeoenvironmental analysis of mass extinction events. *Palaeogeogr. Palaeoclimatol. Palaeoecol.* **2006**, *232*, 190–213. [\[CrossRef\]](#)
96. Li, L.; Keller, G. Maastrichtian climate, productivity and faunal turnovers in planktic foraminifera in South Atlantic DSDP sites 525A and 21. *Mar. Micropaleontol.* **1998**, *33*, 55–86. [\[CrossRef\]](#)
97. Li, L.; Keller, G. Abrupt deep-sea warming at the end of the Cretaceous. *Geology* **1998**, *26*, 995–998. [\[CrossRef\]](#)
98. Abramovich, S.; Keller, G. Planktonic foraminiferal response to the latest Maastrichtian abrupt warm event: A case study from South Atlantic DSDP Site 525A. *Mar. Micropaleontol.* **2003**, *48*, 225–249. [\[CrossRef\]](#)
99. Twitchett, R.J. Incompleteness of the Permian–Triassic fossil record: A consequence of productivity decline? *Geol. J.* **2001**, *36*, 341–353. [\[CrossRef\]](#)
100. Castle, J.W.; Rodgers, J.H., Jr. Hypothesis for the role of toxin-producing algae in Phanerozoic mass extinctions based on evidence from the geologic record and modern environments. *Environ. Geosci.* **2009**, *16*, 1–23. [\[CrossRef\]](#)
101. Jiang, S.; Bralower, T.J.; Patzkowsky, M.E.; Kump, L.R.; Schueth, J.D. Geographic controls on nannoplankton extinction across the Cretaceous/Palaeogene boundary. *Nat. Geosci.* **2010**, *3*, 280–285. [\[CrossRef\]](#)
102. Schueth, J.D.; Bralower, T.J.; Jiang, S.; Patzkowsky, M.E. The role of regional survivor incumbency in the evolutionary recovery of calcareous nannoplankton from the Cretaceous/Paleogene (K/Pg) mass extinction. *Paleobiology* **2015**, *41*, 661–679. [\[CrossRef\]](#)
103. Brinkhuis, H.; Bujak, J.P.; Smit, J.; Versteegh, G.J.M.; Visscher, H. Dinoflagellate-based sea surface temperature reconstructions across the Cretaceous–Tertiary boundary. *Palaeogeogr. Palaeoclimatol. Palaeoecol.* **1998**, *141*, 67–83. [\[CrossRef\]](#)
104. MacLeod, N.; Keller, G. Comparative biogeographic analysis of planktic foraminiferal survivorship across the Cretaceous/Tertiary (K/T) boundary. *Paleobiology* **2016**, *20*, 143–177. [\[CrossRef\]](#)
105. Pardo, A.; Adatte, T.; Keller, G.; Oberhänsli, H. Paleoenvironmental changes across the Cretaceous–Tertiary boundary at Koshak, Kazakhstan, based on planktic foraminifera and clay mineralogy. *Palaeogeogr. Palaeoclimatol. Palaeoecol.* **1999**, *154*, 247–273. [\[CrossRef\]](#)
106. Raup, D.M.; Sepkoski, J.J. Mass Extinctions in the Marine Fossil Record. *Science* **1982**, *215*, 1501–1503. [\[CrossRef\]](#)
107. Paul, C.R.C. Interpreting bioevents: What exactly did happen to planktonic foraminifers across the Cretaceous–Tertiary boundary? *Palaeogeogr. Palaeoclimatol. Palaeoecol.* **2005**, *224*, 291–310. [\[CrossRef\]](#)

108. Keller, G. The end-cretaceous mass extinction in the marine realm: Year 2000 assessment. *Planet. Space Sci.* **2001**, *49*, 817–830. [[CrossRef](#)]
109. MacLeod, N. Impacts and marine invertebrate extinctions. *Geol. Soc. Lond. Spec. Publ.* **1998**, *140*, 217–246. [[CrossRef](#)]
110. Alegret, L.; Molina, E.; Thomas, E. Benthic foraminiferal turnover across the Cretaceous/Paleogene boundary at Agost (south-eastern Spain): Paleoenvironmental inferences. *Mar. Micropaleontol.* **2003**, *48*, 251–279. [[CrossRef](#)]
111. Coccioni, R.; Marsili, A. The response of benthic foraminifera to the K–Pg boundary biotic crisis at Elles (northwestern Tunisia). *Palaeogeogr. Palaeoclimatol. Palaeoecol.* **2007**, *255*, 157–180. [[CrossRef](#)]
112. Coccioni, R.; Galeotti, S. What happened to small benthic foraminifera at the Cretaceous/Tertiary boundary? *Bull. Soc. Geol. Fr.* **1998**, *169*, 271–279.
113. D'Hondt, S.; Donaghay, P.; Zachos, J.C.; Luttenberg, D.; Lindinger, M. Organic Carbon Fluxes and Ecological Recovery from the Cretaceous-Tertiary Mass Extinction. *Science* **1998**, *282*, 276–279. [[CrossRef](#)]
114. Barrera, E.; Keller, G. Productivity across the Cretaceous/Tertiary boundary in high latitudes. *GSA Bull.* **1994**, *106*, 1254–1266. [[CrossRef](#)]
115. Birch, H.S.; Coxall, H.K.; Pearson, P.N.; Kroon, D.; Schmidt, D.N. Partial collapse of the marine carbon pump after the Cretaceous-Paleogene boundary. *Geology* **2016**, *44*, 287–290. [[CrossRef](#)]
116. Zachos, J.C.; Arthur, M.A.; Dean, W.E. Geochemical evidence for suppression of pelagic marine productivity at the Cretaceous/Tertiary boundary. *Nature* **1989**, *337*, 61–64. [[CrossRef](#)]
117. Coxall, H.K.; D'Hondt, S.; Zachos, J.C. Pelagic evolution and environmental recovery after the Cretaceous-Paleogene mass extinction. *Geology* **2006**, *34*, 297–300. [[CrossRef](#)]
118. Schulte, P.; Alegret, L.; Arenillas, I.; Arz, J.A.; Barton, P.J.; Bown, P.R.; Bralower, T.J.; Christeson, G.L.; Claeys, P.; Cockell, C.S.; et al. The Chicxulub Asteroid Impact and Mass Extinction at the Cretaceous-Paleogene Boundary. *Science* **2010**, *327*, 1214–1218. [[CrossRef](#)] [[PubMed](#)]
119. D'Hondt, S.; Herbert, T.D.; King, J.; Gibson, C. Planktic foraminifera, asteroids, and marine production: Death and recovery at the Cretaceous-Tertiary boundary. In *The Cretaceous-Tertiary Event and Other Catastrophes in Earth History*; Ryder, G., Fastovsky, D.E., Gartner, S., Eds.; Geological Society of America: Boulder, CO, USA, 1996; Volume 307.
120. Smith, A.B.; Jeffery, C.H. Selectivity of extinction among sea urchins at the end of the Cretaceous period. *Nature* **1998**, *392*, 69–71. [[CrossRef](#)]
121. Brett, C.E.; Brookfield, M.E. Morphology, faunas and genesis of ordovician hardgrounds from Southern Ontario, Canada. *Palaeogeogr. Palaeoclimatol. Palaeoecol.* **1984**, *46*, 233–290. [[CrossRef](#)]
122. Adams, C.G. Neogene larger foraminifera, evolutionary and geological events in the context of datum planes. In *Pacific Neogene Datum Planes*; University of Tokyo Press: Tokyo, Japan, 1984; pp. 47–68.
123. Karakitsios, V.; Tsikos, H.; Van Breugel, Y.; Bakopoulos, I.; Koletti, L. Cretaceous Oceanic Anoxic events in western continental Greece. *Bull. Geol. Soc. Greece* **2004**, *36*, 846–855. [[CrossRef](#)]
124. Getsos, K.; Pomoni-Papaioannou, F.; Zelilidis, A. A carbonate ramp evolution in the transition from the Apulia platform to the Ionian Basin during Early to Late Cretaceous (NW Greece). *Bull. Geol. Soc. Greece* **2007**, *40*, 53–63. [[CrossRef](#)]
125. Spasojevic, S.; Gurnis, M. Sea level and vertical motion of continents from dynamic earth models since the Late Cretaceous. *AAPG Bull.* **2012**, *96*, 2037–2064. [[CrossRef](#)]
126. Miller, K.; Wright, J.; Katz, M.; Browning, J.; Cramer, B.; Wade, B.S.; Mizintseva, S. A view of Antarctic ice-sheet evolution from sea-level and deep-sea isotope changes during the Late Cretaceous–Cenozoic. In *Antarctica: A Keystone in a Changing World*; National Academies Press: Washington, DC, USA, 2008; pp. 55–70.
127. Tsikos, H.; Karakitsios, V.; Breugel, Y.V.; Walsworth-Bell, B.; Bombardiere, L.; Petrizzo, M.R.; Damsté, J.S.S.; Schouten, S.; Erba, E.; Silva, I.P.; et al. Organic-carbon deposition in the Cretaceous of the Ionian Basin, NW Greece: The Paquier Event (OAE 1b) revisited. *Geol. Mag.* **2004**, *141*, 401–416. [[CrossRef](#)]
128. Tucker, M.E. *Sedimentary Petrology: An Introduction to the Origin of Sedimentary Rocks*; John Wiley & Sons: Hoboken, NJ, USA, 2009.
129. Wilson, M.E.J.; Moss, S.J. Cenozoic palaeogeographic evolution of Sulawesi and Borneo. *Palaeogeogr. Palaeoclimatol. Palaeoecol.* **1999**, *145*, 303–337. [[CrossRef](#)]
130. Janjuhah, H.T.; Alansari, A.; Santha, P.R. Interrelationship Between Facies Association, Diagenetic Alteration and Reservoir Properties Evolution in the Middle Miocene Carbonate Build Up, Central Luconia, Offshore Sarawak, Malaysia. *Arab. J. Sci. Eng.* **2019**, *44*, 341–356. [[CrossRef](#)]
131. Flügel, E. *Microfacies Analysis of Limestones*; Springer Science & Business Media: Berlin/Heidelberg, Germany, 2012.
132. Hoang, A.N. Diagenetic evolution recorded from the fractured carbonates of Trang Kenh formation, in the north-eastern area of Vietnam. *Petrovietnam J.* **2017**, *6*, 20–28.